in cell proliferation but also in cell differentiation. The effect of extracellular matrix (ECM) proteins such as collagen type I, collagen type IV, gelatin, laminin, fibronectin, Matrigel (a mixture of laminin, collagen type IV, heparan sulfate proteoglycans, and entactin), and Cardiogel (a mixture of collagen types I and III, glycoproteins, laminin, fibronectin, and proteoglycans) on cell viability, proliferation rate, and cardiomyocyte gene expression have been reported;[10,11] however, the cardiomyocyte beating behavior has not fully been discussed.

In the present study, differentiation to beating cardiomyocytes and the beating duration of the cardiomyocytes were studied using two types of model cells. Murine embryonal carcinoma (EC) stem cells (P19.CL6),[12] which are widely used for investigating cardiac differentiation, were treated with differentiation medium containing 1% dimethyl sulfoxide (DMSO) on various ECM proteins (collagen, type I gelatin, and fibronectin), and their differentiation efficiency was evaluated. The effect of these substrates on the beating duration of rat neonatal cardiomyocytes was also investigated, along with intracellular cardiac marker genes [troponin T type-2 (TNNT2) and troponin C type-1 (TNNC1)][13] and skeletal muscle marker gene [troponin C type-2 (TNNC2)], which is reported to be expressed in the early developing heart.[14] Any fundamental information obtained would be important for the cardiac differentiation of various stem cells, including autologous BMSCs.

Materials and methods

Cardiomyocytes

Cardiomyocytes were isolated from neonatal Sprague–Dawley rat heart (1 to 2 days old) by the collagenase digestion method with modifications.[15,16] Institutional guidelines for the care and use of laboratory animals were observed. The hearts were removed and carefully minced with a scalpel blade into fragments and were rinsed several times with Hanks' balanced salt solution (Sigma-Aldrich, St. Louis, MO, USA) to remove blood and cellular debris. The minced hearts were gently stirred in 50 ml collagenase solution [0.15 M Sodium Chloride (NaCl), 5.63 mM Potassium Chloride (KCl), 0.02 M 4-(2-hydroxyethyl)-1-piperazineethanesulfonic acid (HEPES), 0.02 M Sodium Hydrogen Carbonate ($NaHCO_3$), 3.74 mM Calcium Chloride Dihydrate ($CaCl_2{\cdot}2H_2O$), and 6.5×10^4 U collagenase (Wako, Osaka, Japan, Lot no: 06032W)] at 37°C for 30 min. The resulting cell suspension was filtered through a nylon cell strainer (BD Falcon, BD Biosciences, Bedford, MA, USA) with a 40-μm pore size and centrifuged at 78 g for 3 min.

Isolated cardiomyocytes (1.0×10^5) were cultured in minimum essential medium alpha medium (α-MEM, Gibco, Invitrogen, Grand Island, NY, USA) supplemented with 10% (v/v) fetal bovine serum (FBS, MP Biomedicals, Eschwege, Germany, lot no: 7297H), and 100 IU/l penicillin–streptomycin (Wako, Osaka, Japan) on 60-mm gelatin- (IWAKI, Asahi Glass, Tokyo, Japan), fibronectin-(BD Falcon, BD BioCoat, BD Biosciences), or collagen type I-coated dishes and noncoated polystyrene dishes (IWAKI).

Differentiation of P19.CL6 cells

Differentiation of P19.CL6 cells was performed as described by Ohkubo with modifications.[12] Briefly, P19.CL6 cells were plated at a density of 3.7×10^5 cells on 60-mm gelatin-, fibronectin-, or collagen type I-coated dishes or noncoated polystyrene dishes with a α-MEM supplemented with 10% (v/v) FBS containing 1% DMSO (Wako). As a control experiment, P19.CL6 cells were cultured with α-MEM supplemented with 10% (v/v) FBS without 1% DMSO. The medium was changed every 2 days.

Measurement of action potential

Cultured plates on which beating colonies appeared were placed on the stage of an inverted phase-contrast optical microscope (ZEISS, Axiovert 135, Munich, Germany) and action potentials were measured immediately by a conventional microelectrode. The measurements were conducted after 1, 2, and 3 weeks of cultivation. Silicon-coated Ag wire (A-M System, Carlsborg, WA, USA, 250 μm bare, 330 μm coated) was used as the microelectrode. The microelectrode was set in a micromanipulator system (MON-202D, Nikon Narishige, Tokyo, Japan) and connected to a bioelectric amplifier (AB-621G, Nihon Kohde, Osaka, Japan). The sensitivity and time constant of the bioelectric amplifier were set at 0.1 mV/div and 0.003 s. For the measurements, the microelectrode was adjusted using the micromanipulator until it was attached to the membrane of beating cells. The voltage difference was amplified by the bioelectric amplifier and was displayed and recorded using Chart 5 software (AD Instrument, Bella Vista, Australia).

Total RNA isolation and reverse transcription

Total RNAs of cardiomyocytes and DMSO-treated P19.CL6 cells cultured on various dishes were extracted by QuickGene RNA cultured cell kit S (Fujifilm Life Science, Tokyo, Japan) 4 weeks after culture and 11 days after culture, respectively.

First-strand cDNAs were synthesized using a mixture of oligo$(dT)_{18}$ primer. Total cellular RNAs (200 ng) were incubated with 2.5 μM oligo$(dT)_{18}$ primer at 70°C for 10 min to denature the RNA secondary structure and then incubated at 4°C to let the primer anneal to the RNA. A given amount of 5X RT buffer (Toyobo, Osaka, Japan) and 2.5 mM Deoxynucleotide Trisphasphate (dNTP) mixture (Takara Bio, Shiga, Japan) (4 μl) were added and incubated at 37°C for 5 min. The reverse transcriptase (100 Units, Toyobo) was added into the mixture and the reverse transcriptase (RT) reaction was extended at 37°C for 1 h. Then, the reac-

Table 1. Polymerase chain reaction primers used in this study

Genes	Sense	Antisense
TNNT2	5′-GAAACAGGATCAACGACAACCA-3′	5′-CGCCCGGTGACTTTGG-3′
TNNC1	5′-GATCTCTTCCGCATGTTTGACA-3′	5′-TGGCCTGCAGCATCATCTT-3′
TNNC2	5′-AGATCGAATCCCTGATGAAGGA-3′	5′-CATCTTCAGAAACTCGTCGAAGTC-3′
GAPDH	5′-CTACCCCCAATGTATCCGTTGT-3′	5′-TAGCCCAGGATGCCCTTTAGT-3′

GAPDH, Glyceraldehyde 3 phosphate dehydrogenase

Table 2. Summary of voltage potentials for cardiomyocytes cultured in several types of extracellular matrix-coated dishes

Substrate	Action potential (mV) [Beating rate (Hz)]		
	Day 7	Day 14	Day 21
Gelatin	6.7 ± 0.49 [1.2 ± 0.05]	6.6 ± 1.26 [1.3 ± 0.01]	3.1 ± 0.21[2.8 ± 0.03]
Fibronectin	1.1 ± 0.97 [1.1 ± 0.30]	6.9 ± 1.15 [1.3 ± 0.42]	2.8 ± 0.11[2.0 ± 0.11]
Collagen type-I	2.6 ± 0.35 [0.8 ± 0.02]	1.7 ± 0.03 [2.3 ± 0.05]	ND
Polystyrene	2.0 ± 0.75 [0.3 ± 0.04]	ND	ND

ND, not done

tion mixture was heated at 94°C for 5 min to inactivate the enzyme and cooled at 4°C for 15 min. The RNase (DNase-free, 0.5 μg, Roche Diagnostics, Mannheim, Germany) was added to the mixture and incubated at 37°C to remove the template of RNA.

Real-time quantitative polymerase chain reaction

Real-time quantitative polymerase chain reaction (PCR) was conducted with SYBR Green. Primers for PCR analysis for troponin T type-2, troponin C type-1, and troponin C type-2 were designed using Primer Express software (Perkin-Elmer Applied Biosystems, Warrington, UK). The primer sequences are shown in Table 1. The reaction mixtures contained 23.74 μl distilled water, 25 μl SYBR Green Realtime PCR master mix (Toyobo), 100 nM of each primer, and 0.26 μl cDNA. The thermal profile for PCR was 50°C for 2 min, followed by 95°C for 10 min, followed by 40 cycles of 15 s at 95°C and 1 min at 60°C. Distilled water 0.26 μl was used as a negative control PCR reaction to ensure the absence of template contamination in PCR reagents. The average threshold cycle (Ct) values of triplicate measurements were used for all subsequent calculations on the basis of the delta Ct method.

Results

Beating behavior of isolated cardiomyocytes

One week after culture, the action potential of cardiomyocytes on gelatin-coated dishes was higher than that for other conditions (Fig. 1), and the beating duration was also longer than that for other conditions. The action potential and beating rates on each matrix are summarized in Table 2. After 7 days of culture, the action potential was around 6.7 ± 0.49 mV for cardiomyocytes cultured on gelatin-coated dishes, 1.1 ± 0.97 mV on fibronectin-coated dishes, 2.0 ± 0.35 mV on collagen type I-coated dishes, and 2.0 ± 0.75 mV on noncoated polystyrene dishes. These results indicate that the beating rate on fibronectin-coated dishes, collagen type I-coated dishes, and noncoated polystyrene dishes were 84%, 61%, and 70% lower than the beating rate on gelatin-coated dishes after 1 week of cultivation.

After 14 days of culture, the action potential became 6.6 ± 1.26 mV on gelatin-coated dishes, 6.9 ± 1.15 mV on fibronectin-coated dishes, and 1.7 ± 0.03 mV on collagen type I-coated dishes. No beating was observed on noncoated polystyrene dishes after 2 weeks of cultivation. After 21 days of culture, the action potential was 3.1 ± 0.21 mV on gelatin-coated and 2.8 ± 0.11 mV on fibronectin-coated dishes. No action potential was detected on collagen type I-coated dishes and polystyrene dishes.

The beating rate of cardiomyocytes was also affected by the ECM proteins. After 7 days of culture, the beating rate of cardiomyocytes was 1.2 ± 0.05 Hz on gelatin-coated dishes, 1.1 ± 0.3 Hz on fibronectin-coated dishes, 0.8 ± 0.02 Hz on collagen type I-coated dishes, and 0.3 ± 0.04 Hz on noncoated polystyrene dishes. After 14 days of culture, the beating rate became 1.3 ± 0.01 Hz on gelatin-coated dishes, 1.3 ± 0.42 Hz on fibronectin-coated dishes, and 2.3 ± 0.05 Hz on collagen type I-coated dishes. After 21 days, the beating rate was 2.8 ± 0.03 Hz on gelatin-coated dishes and 2.0 ± 0.11 Hz on fibronectin-coated dishes, whereas cardiomyocytes cultured on noncoated polystyrene dishes and collagen-coated dishes did not beat well and stopped at an early stage of cultivation. These results indicate that gelatin could maintain the beating behavior of cardiomyocytes for a longer time compared to fibronectin or collagen type I.

Expression of troponin T type-2 and troponin C type-1

Cardiac troponin T type-2 and troponin C type-1 are known to be cardiomyocyte markers and are important in the structure of muscle tissue; they also play a role in the contraction of muscle cells.[13] After 4 weeks of culture,

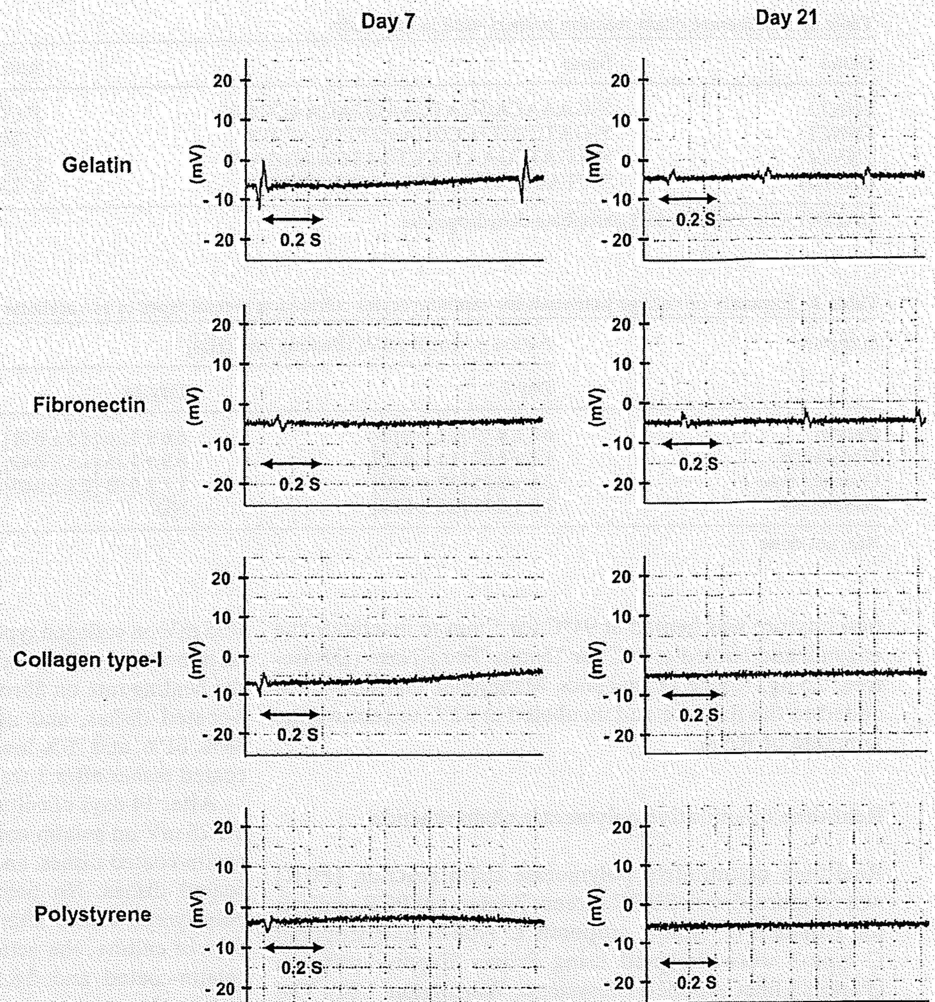

Fig. 1. Electrophysiological assessment of isolated cardiomyocytes after 7 and 21 days of cultivation on different substrates

expression of troponin T type-2 in cardiomyocytes on gelatin-coated dishes was 7, 6, and 12 times higher than those on fibronectin-coated, collagen-coated, and non-coated dishes (Fig. 2A). Expression of troponin C type-1 on gelatin-coated dishes was also 5, 6, and 32 times higher than those on fibronectin-coated, collagen type I-coated, and noncoated dishes (Fig. 2B). These results are consistent with the results of the electrophysiological study (Fig. 1), in which the beating of cardiomyocytes still could be detected on gelatin- and fibronectin-coated dishes after 3 weeks of cultivation.

Differentiation of P19.CL6 cells

Beating colonies were found on gelatin-coated dishes in 9 days with α-MEM medium containing 1% DMSO. This was followed by cells cultured on fibronectin-coated dishes after 10 days of culture and collagen type I-coated dishes after 11 days of culture. The average number of beating colonies found on the first day of detection was 13 ± 7 colonies per dish on gelatin-coated dishes, 9 ± 5 colonies per dish on fibronectin-coated dishes, 5 ± 2 colonies on collagen type I-coated dishes, and 3 ± 1 colonies on polystyrene dishes (Table 3).

As described earlier, troponin T type-2 and troponin C type-1 are known to be markers of cardiomyocytes,[13] and troponin C type-2 is reported to be a marker of cardiac development.[14] Expression of troponin T type 2 on gelatin- and fibronectin-coated dishes was higher than that for the other dishes, as shown in Fig. 3A. However, the expression of troponin C type-2 in collagen type I-coated dishes and noncoated polystyrene dishes was higher than that in gelatin- and fibronectin-coated dishes. The high expression of troponin C type-2 on collagen type I coated dishes and noncoated polystyrene dishes on day 11 was possibly because of the delayed differentiation of P19.CL6 cells to cardiomyocytes-like cells. Stoutamyer and Dhoot reported that troponin C type-2 was first expressed on day 3, reached maximum expression on day 5, and decreased day by day until no expression was found on day 11 during the development of quail heart in ovo.[14] Stoutamyer and Dhoot also reported that the expression of troponin C type-1 was detected on day 2 and decreased during the increase of

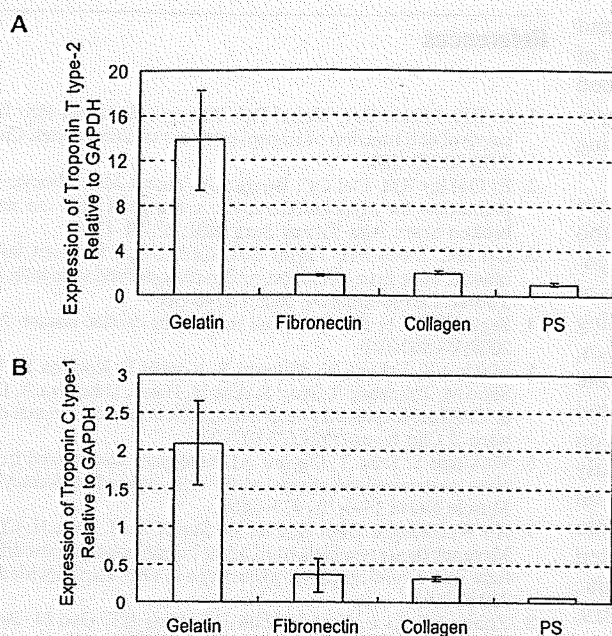

Fig. 2. Expression of cardiac markers (**A** troponin T type-2 and **B** troponin C type-1) in isolated cardiomyocytes after cultivation for 4 weeks on various types of extracellular matrix. *GAPDH*, Glyceraldehyde 3 phosphate dehydrogenase; *PS*, polystyrene

Table 3. Number of beating colonies of P19.CL6 cells 11 days after induction with 1% dimethyl sulfoxide

Substrate	Average number of beating colonies per dish
Gelatin	13 ± 7
Fibronectin	9 ± 5
Collagen type-I	5 ± 2
Polystyrene	3 ± 1

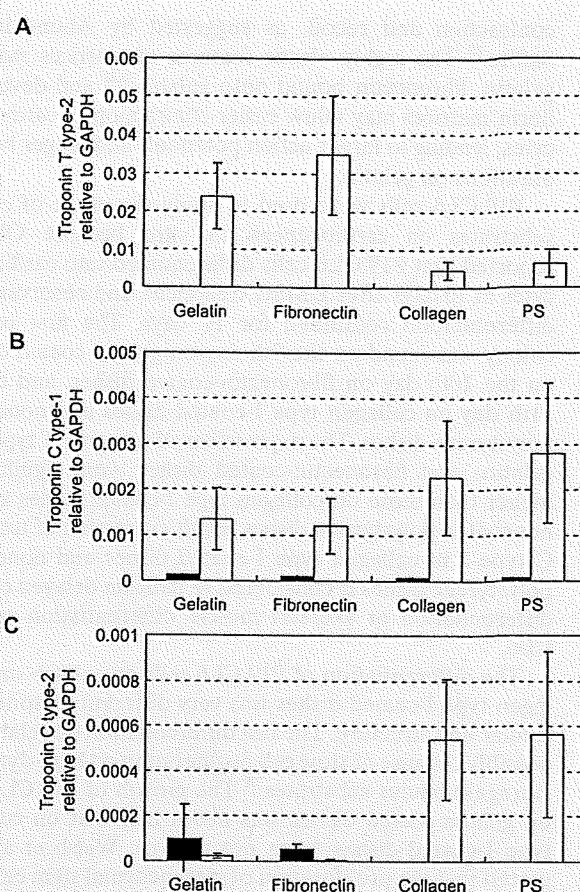

Fig. 3. Expression of cardiac markers in P19.CL6 cells (**A** troponin T type-2, **B** troponin C type-1, **C** troponin C type-2) treated with minimum essential medium alpha medium (α-MEM) containing 1% dimethyl sulfoxide on various dishes (*white bars*) or with α-MEM as a control for 11 days (*black bars*) PS, polysyrene

troponin C type-2, reaching a constant level after that.[14] In addition, the troponin C type-2 expression on a collagen-coated or noncoated dish may suggest skeletal muscle differentiation of P19.CL6 cells, although further analysis is needed.

These results demonstrated that differentiation of P19. CL6 cells to beating cells on gelatin-coated dishes and fibronectin-coated dishes was faster and more effective than that on collagen type I-coated dishes and noncoated polystyrene dishes.

Discussion

In the present study, enhanced action potentials and elongated beating durations of neonatal cardiomyocyte were observed on gelatin-coated dishes compared to those on collagen type I-coated dishes. Possible differences between gelatin and collagen are: (1) collagen posses a triple-helical conformation, (2) gelatin has a wide molecular weight distribution depending on its preparation process, (3) gelatin is easily hydrolyzed by protease,[17] (4) the dynamic storage modulus of gelatin is higher than that of collagen,[18] and (5) gelatin binds with fibronectin with a higher affinity.[19–21] It has already been reported that fibronectin is a very elastic substrate.[22]

The mechanism of the elongated beating duration on gelatin-coated substrate is unclear, but the mechanical properties (elasticity) and biological activity of the substrates might be influential. It has been reported that the mechanical properties of culture matrices affect various cellular properties such as the morphology of embryonic stem cells,[23,24] the collagen production of fibroblasts,[25,26] and the differentiation of mesenchymal and neural stem cells.[27,28]

Fibronectin produced by culture cells is known to associate with the fibronectin-binding domain of collagen, resulting in fibrillogenesis.[21] It has also been reported that fibronectin binds to gelatin more strongly than to collagen.[20,21] Therefore, the high production of fibrils might occur more effectively on gelatin-coated dishes than on fibronectin- or collagen-coated dishes. These connecting elastic fibers might regulate the motion of cardiomyocytes during

contraction and recoil, as suggested by Ahumada and Saffitz.[29] The highly elastic features of matrices made of gelatin, fibronectin bound onto gelatin,[18,22] and developed fibrin matrices may allow easier contraction of cardiomyocytes, leading to larger action potentials and longer beating durations on gelatin.

P19.CL6 cells were used to study the effect of culture substrates on cardiogenesis in vitro because Ohkubo reported that P19.CL6 cells differentiated into cardiomyocytes in 10 days after DMSO treatment, and observation of differentiation continued for 11 days. The first beating colony was found on the 9th day on gelatin-coated dishes, on the 10th day on fibronectin-coated dishes, and on the 11th day on collagen type I-coated dishes and noncoated polystyrene dishes. The expressions of troponin T type-2 on gelatin- and fibronectin-coated dishes were significantly higher than those on collagen type I-coated dishes and on noncoated polystyrene dishes. High expression of troponin C type-2 in collagen type I-coated dishes and noncoated polystyrene dishes is considered to indicate delayed cardiac differentiation or skeletal muscle differentiation of P19.CL6.

The differentiation of P19.CL6 cells on gelatin- and collagen type I-coated dishes was very different, despite their similar unit structure. The fast differentiation on gelatin was possibly because of slow cell proliferation on high-dynamic-storage-modulus substrates.[18] The growth of P19.CL6 cells on gelatin-coated dishes was about half that on collagen type I-coated dishes (data not shown). Walsh et al. suggested that the proliferation of mesenchymal stem cells was suppressed during the differentiation to osteoblasts in vitro.[30] The fast differentiation on fibronectin-coated dishes may also relate to the elasticity of the substrate.[22]

This finding will hopefully offer a bright future for the myocardial patch scaffold. It has been reported that the probability of cardiac differentiation of adipose tissue-derived mesenchymal stem cells after transplantation to infracted rat heart is quite low.[31] In the present study, the gelatin-based niche was found to be preferable for cardiac differentiation and for the beating function of cardiomyocytes. We will be applying these results to the cardiac differentiation of mesenchymal stem cells in order to prepare allogeneic beating cardiomyocytes.

Conclusion

The physical and biological properties of the substrate were the important factors not only for maintaining cardiac functions but also for leading to the cardiac differentiation of P19.CL cells. Gelatin was found to be a promising ECM protein to this end in vitro.

Acknowledgments This work was partly supported by a Grant-in-Aid for Scientific Research (B) from the Ministry of Education, Culture, Sports, Science and Technology of Japan. The author (Azizi Miskon) would like to thank the Ministry of Higher Education, Malaysia, and Tun Hussein Onn of the University of Malaysia for funding his study under the Academic Training Scheme.

References

1. Li RK, Mickle DA, Weisel RD, Zhang J, Mohabeer MK. In vivo survival and function of transplanted rat cardiomyocytes. Circ Res 1996;78:283–288
2. El Oakley RM, Ooi OC, Bongso A, Yacoub MH. Myocyte transplantation for myocardial repair: a few good cells can mend a broken heart. Ann Thorac Surg 2001;71:1724–1733
3. Ott HC, Davis BH, Taylor DA. Cell therapy for heart failure – muscle, bone marrow, blood, and cardiac-derived stem cells. Semin Thorac Cardiovasc Surg 2005;17:348–360
4. Segers VF, Lee RT. Stem-cell therapy for cardiac disease. Nature 2008;451:937–942
5. Makino S, Fukuda K, Miyoshi S, Konishi F, Kodama H, Pan J, Sano M, Takahashi T, Hori S, Abe H, Hata J, Umezawa A, Ogawa S. Cardiomyocytes can be generated from marrow stromal cells in vitro. J Clin Invest 1999;103:697–705
6. Wakitani S, Saito T, Caplan AI. Myogenic cells derived from rat bone marrow mesenchymal stem cells exposed to 5-azacytidine. Muscle Nerve 1995;18:1417–1426
7. Xu W, ZhangX, Qian H, Zhu W, Sun X, Hu J, Zhou H, Chen Y. Mesenchymal stem cells from adult human bone marrow differentiate into a cardiomyocyte phenotype in vitro. Exp Biol Med 2004; 229:623–631
8. Zhang FB, Li L, Fang B, Zhu DL, Yang HT, Gao PJ. Passage-restricted differentiation potential of mesenchymal stem cells into cardiomyocyte-like cells. BBRC 2005;336:784–792
9. Liu Y, Song J, Liu W, Wan Y, Chen X, Hu C. Growth and differentiation of rat bone marrow stromal cells: does 5-azacytidine trigger their cardiomyogenic differentiation? Cardiovasc Res 2003;58:460–468
10. Macfelda K, Kapeller B, Wilbacher I, Losert UM. Behavior of cardiomyocytes and skeletal muscle cells on different extracellular matrix components – relevance for cardiac tissue engineering. Artif Organs 2007;31:4–12
11. Bird SD, Doevendans PA, van Rooijen MA, Brutel de la Riviere A, Hassink RJ, Passier R, Mummery CL. The human adult cardiomyocyte phenotype. Cardiovasc Res 2003;58:423–434
12. Ohkubo AH. Differentiation of beating cardiac muscle cells from a derivative of P19 embryonal carcinoma cells. Cell Struct Funct 1996;21:101–110
13. Saggin L, Ausoni S, Gorza L, Sartore S, Schiaffino S. Troponin T switching in the developing rat heart. J Biol Chem 1998;263: 18488–18492
14. Stoutamyer A, Dhoot GK. Transient expression of fast troponin C transcripts in embryonic quail heart. J Muscle Res Cell Motil 2005;26:237–245
15. Seglen PO. Preparation of isolated rat liver cells. Methods Cell Biol 1976;13:29–83
16. Moldeus P, Högberg J, Orrenius S. Isolation and use of liver cells. Methods Enzymol 1978;52:60–71
17. Zhang Z, Li G, Shi B. Physicochemical properties of collagen, gelatin, and collagen hydrolysate derived from bovine limed split wastes. J Soc Leather Technol Chem 2006;90:23–28
18. Chien JC, Chang EP. Dynamic mechanical and rheo-optical studies of collagen and gelatin. Biopolymers 1972;11:2015–2031
19. Little CD, Chen WT. Masking of extracellular collagen and the co-distribution of collagen and fibronectin during matrix formation by cultured embryonic fibroblast. J Cell Sci 1982;55: 35–50
20. Engvall E, Ruoslahti E, Miller ED. Affinity of fibronectin to collagens of different genetic types and to fibrinogen. J Exp Med 1978;147:1584–1595
21. Dzamba BJ, Wu H, Jaenisch R, Peters DM. Fibronectin binding site in type I collagen regulates fibronectin fibril formation. J Cell Biol 1993;121:1165–1172
22. Erickson HP. Stretching fibronectin. J Muscle Res Cell Motil 2002;23:575–580
23. Bard JB, Hay ED. The behavior of fibroblasts from the developing avian cornea. Morphology and movement in situ and in vitro. J Cell Biol 1975;67:400–418
24. Hay ED. Interaction of embryonic surface and cytoskeleton with extracellular matrix. Am J Anat 1982;165:1–12

25. Nakagawa S, Pawelek P, Grinnell F. Extracellular matrix organization modulates fibroblast growth and growth factor responsiveness. Exp Cell Res 1989;182:572–582
26. Halliday NL, Tomasek JJ. Mechanical properties of the extracellular matrix influence fibronectin fibril assembly in vitro. Exp Cell Res 1995;217:109–117
27. Engler AJ, Sen S, Sweeney HL, Discher DE. Matrix elasticity directs stem cell lineage specification. Cell 2006;126:677–689
28. Saha K, Keung AJ, Irwin EF, Li Y, Little L, Schaffer DV, Healy KE. Substrate modulus directs neural stem cell behavior. Biophys J 2008;95:4426–4438
29. Ahumada GG, Saffitz JE. Fibronectin in rat heart: a link between cardiac myocytes and collagen. J Histochem Cyotchem 1984;4: 383–388
30. Walsh S, Jordan GR, Jefferiss C, Stewart K, Beresford JN. High concentrations of dexamethasone suppress the proliferation but not the differentiation or further maturation of human osteoblast precursors in vitro: relevance to glucocorticoid-induced osteoporosis. Rheumatology 2001;40:74–83
31. Miyahara Y, Nagaya N, Kataoka M, Yanagawa B, Tanaka K, Hao H, Ishino K, Ishida H, Shimizu T, Kangawa K, Sano S, Okano T, Kitamura S, Mori H. Monolayered mesenchymal stem cells repair scarred myocardium after myocardial infarction. Nat Med 2006;12: 459–465

In Vivo Tissue Response and Degradation Behavior of PLLA and Stereocomplexed PLA Nanofibers

Daisuke Ishii,[†,‡] Tang Hui Ying,[†,§,∥] Atsushi Mahara,[⊥] Sunao Murakami,[⊥] Tetsuji Yamaoka,[⊥] Won-ki Lee,[∇] and Tadahisa Iwata*[,†,○]

Polymer Chemistry Laboratory, RIKEN Institute, 2-1 Hirosawa, Wako-shi, Saitama 351-0198, Japan, School of Biological Science, Universiti Sains Malaysia, 11800 Penang, Malaysia, Department of Biomedical Engineering, Advanced Medical Engineering Center, National Cardiovascular Center Research Institute, 5-7-1 Fujishirodai, Suita, Osaka 565-8565, Japan, and Division of Chemical Engineering, Pukyong National University, San 100, Yongdang-dong, Nam-gu, Busan 608-739, Republic of Korea

Received August 21, 2008; Revised Manuscript Received November 24, 2008

Biocompatibility of PLLA and stereocomplexed PLA nanofibers was evaluated by subcutaneous implantation in rats for 4–12 weeks. Characterization of the nanofibers was performed by GPC, SEM, wide-angle X-ray diffraction, and optical microscopy of hematoxylin-eosin stained ultrathin sections of explanted nanofibers. Stereocomplexed PLA nanofiber showed slower degradation than PLLA nanofiber and thus retained their shape after prolonged implantation. Furthermore, stereocomplexed PLA nanofiber caused milder inflammatory reaction than PLLA nanofiber. These results offer the potential use of PLLA and stereocomplexed PLA nanofibers as a biomaterial for short-term and long-term tissue regeneration, respectively. Stereocomplexed PLA nanofiber after in vitro degradation showed smaller degree of swelling than PLLA nanofiber. Taking the results of in vivo degradation together with in vitro degradation into consideration, bioabsorption mechanism of the in vivo degradation of the nanofibers is proposed.

Introduction

In the field of medical sciences, the method of tissue engineering has been extensively studied to overcome the problems of conventional methods such as organ transplantation and usage of artificial organs.[1] In tissue engineering, the proliferation and differentiation of cultured cells for deficiency repair has to be artificially controlled. The development of scaffold materials on which cells proliferate and differentiate has been a major concern in tissue engineering. Conventionally, collagens and gelatins extracted from animals have been used to produce scaffolds. However, the usage of these animal-origin materials is shrinking for fear of infectious diseases. Alternatively, the usage of biodegradable and biocompatible polymers that do not contain infectious substances such as endotoxins and prions has been explored.

Recently, as a novel method for producing scaffolds, formation of nanofibers with the diameter ranging from several tens to hundreds of nanometers is extensively studied.[2–4] Nanofiber scaffolds have fine pores and grooves as small as a few micrometers wide. Such fine structural features facilitate the adhesion and proliferation of cells. It is required for nanofiber scaffolds to sustain sufficient strength to support regenerating tissue cells and to be degraded after the tissue regeneration is completed. To meet these demands, various kinds of biodegradable and biocompatible polymers have been processed into nanofibers. Furthermore, the fiber morphology, crystalline structure, and degradation behavior of the nanofibers have been investigated.[5–7]

Poly(lactide) (PLA) is one of a few polymers that is practically applied as various medical materials such as implants and sutures.[8] PLA possesses mechanical properties sufficient to endure the mechanical load applied in human body. However, it is readily hydrolyzed both in enzymatic and nonenzymatic conditions.[9] The high susceptibility of PLA toward hydrolysis becomes a shortcoming when the long-time storage under physiological conditions is required. Various efforts to overcome this shortcoming have been attempted. One of such efforts is the formation of stereocomplex in PLA materials.

Stereocomplexed PLA is a characteristic crystalline form of PLA.[10,11] A sterically stable racemic crystal of stereocomplexed PLA is formed by complexing poly(L-lactide) (PLLA) and poly(D-lactide) (PDLA) that take molecular conformations of left-handed and right-handed helices, respectively.[12] As a result, stereocomplexed PLA has a melting temperature of 230 °C, that is 50 °C higher than PLLA and PDLA.[10] Furthermore, it has been reported that stereocomplexed PLA is more stable against hydrolysis than PLLA.[13–15] This finding offers the possibility for controlling the hydrolytic behavior of PLA material by the formation of stereocomplex. Although various methods have been proposed and investigated for the formation of stereocomplex within PLA materials,[16,17] PLA materials that contain only racemic crystal has not yet been processed. Furthermore, the conventional processes involve long-time annealing at elevated temperatures as high as 180 °C and repeated stretching. To form stereocomplexed PLA more conveniently, electrospinning has recently been applied to the formation of stereocomplexed

* To whom correspondence should be addressed. Tel.: +81-3-5841-7888. Fax: +81-3-5841-1304. E-mail: atiwata@mail.ecc.u-tokyo.ac.jp.
† RIKEN Institute.
‡ Present affiliation and address: Department of Materials Chemistry, Faculty of Science and Technology, Ryukoku University 1-5 Yokotani, Seta Oe-cho, Otsu-shi, Shiga 520-2194, Japan.
§ Universiti Sains Malaysia.
∥ Present affiliation and address: Bioengineering Laboratory, RIKEN Institute, 2-1 Hirosawa, Wako-shi, Saitama 351-0198, Japan.
⊥ National Cardiovascular Center Research Institute.
∇ Pukyong National University.
○ Present affiliation and address: Graduate School of Agricultural and Life Sciences, The University of Tokyo, 1-1-1 Yayoi, Bunkyo-ku, Tokyo 113-8657, Japan.

10.1021/bm8009363 CCC: $40.75 © 2009 American Chemical Society
Published on Web 12/31/2008

PLA.[18] In particular, we have first succeeded in processing stereocomplexed PLA nanofiber in which the racemic crystal is only the crystalline polymorph.[19] The formation of racemic crystal was performed by annealing the as-spun nanofiber at 100 °C, which is 80 °C lower than those in previously reported studies.

The degradation behavior of PLA nanofibers has been investigated by using various specimens and conditions.[20-22] However, the previous reports were all limited to in vitro conditions. There have been no reports on the biocompatibility and in vivo degradation behavior of stereocomplexed PLA nanofibers.

In this work, tissue responses and degradation behavior of PLLA and stereocomplexed PLA nanofibers in vivo were investigated by subcutaneously implanting these nanofibers in rats. The tissue response against the nanofibers has been investigated by means of histological observation. The changes in structure and properties of the nanofibers during subcutaneous implantation has been investigated using scanning electron microscopy (SEM), wide-angle X-ray diffraction (WAXD), gel permeation chromatography (GPC), and mechanical tensile testing. The relation between tissue response and degradation behavior of nanofibers is discussed in terms of the structural and property changes of the nanofibers.

Experimental Section

Materials. PLLA with a M_n of 4.7×10^5 and M_w/M_n of 1.8 was purchased from Polysciences, Inc. and used as received. PDLA with a $M_n = 2.2 \times 10^5$ and M_w/M_n of 1.5 was synthesized according to the following procedure. The D-lactide monomer, obtained from Purac, was recrystallized from anhydrous ethyl acetate. Bulk polymerizations were carried out in glass ampoules containing a magnetic stirring bar at 130 °C. Stannous octanoate in petroleum ether was used as the catalyst for the ring-opening polymerization. The ampoules were evacuated using a high vacuum pump and repeatedly flushed with high purity nitrogen to remove volatile impurities, solvents, and oxygen. Then the ampoules were sealed with a blowtorch and heated to the reaction temperature. The products in the ampoules were dissolved in chloroform, precipitated in the excess of methanol, filtered, and dried.

Electrospinning. Solutions of PLLA and PDLA (1 wt %) were prepared using 1,1,1,3,3,3-hexafluoro-2-propanol, HFIP, as the solvent. For the preparation of PLA stereocomplex nanofibers, equal volume of PLLA and PDLA solutions were mixed for several seconds by vortex mixer. Nanofibers were prepared using an Esprayer ES-2000 electrospinning device by Fuence, Co. Ltd. Dope solutions were extruded with a speed of 2.4 mL/h from a syringe needle with an inner diameter of 0.5 mm. Electrical voltage of 15 kV was applied to the syringe. Nanofibers were deposited onto a 10×10 cm^2 aluminum substrate placed perpendicular to the needle. To ensure sufficient thickness of nanofiber mats, the substrate was covered with a template made by a 51.4 μm thick Kapton film on which a 3×3 cm^2 window was opened. Distance between the needle tip and the substrate was set to 15 cm. The atmosphere of the spinning chamber was kept at less than 30% of relative humidity. PLLA and PLA stereocomplex nanofibers were then annealed in an oven at 100 °C for 8 h. Each electrospun PLA nanofiber mats was then cut into two different dimensions measuring 1×1 cm^2 and 1×3 cm^2, respectively. To prevent contamination, all scaffolds were sterilized overnight with ethylene oxide at 40 °C and kept in sealed bags until use.

Subcutaneous Implantation in Rat and Retrieval. Two 12-week old male Wistar rats were used for implanting the scaffolds; one for scaffolds measuring 1×1 cm^2, while the other for scaffolds measuring 1×3 cm^2. The experimental protocol had been approved by the Animal Care Committee of the National Cardiovascular Center, Osaka, Japan. The implantation of nanofiber mat was performed under anesthesia using diethyl ether. The 1×1 cm^2 scaffolds were implanted subcutaneously at one side of the backbone while the 1×3 cm^2 scaffolds were implanted subcutaneously at the backbone. The grouping of the rats was based on the duration of observation for 4 weeks and 12 weeks.

Upon explantation, the nanofiber mats measuring 1×1 cm^2 were excised with the surrounding tissues and stored in 2.5% glutaraldehyde in phosphate buffer saline (PBS) with a pH of 7 until further preparation of ultrathin section for histological observation. The retrieved 1×3 cm^2 nanofiber mats were treated with 1.25 wt % trypsin solution to remove the surrounding tissues. They were then kept in tubes containing PBS at 4 °C until further use. Trace amount of sodium azide was added to avoid the decay of the specimens. After trypsin treatment, surrounding tissues were manually removed as much as possible. The nanofiber mats were repeatedly washed using milli-Q water and dehydrated using ethanol series. Finally, the dehydrated nanofiber mats were dried overnight using vacuum desiccator at room temperature.

In Vitro Degradation. Nanofiber mats with the size of 1×3 cm^2 were incubated in 5 mL of PBS with a pH of 7.27 for 4–12 weeks at 37 °C. The medium was changed every 2 weeks. After 4 and 12 weeks of incubation, the nanofiber mats were washed thoroughly with distilled water, vacuum-dried at room temperature, and then subjected to SEM observation.

Histological Observation. The surrounding tissues were excised together with the implanted nanofiber mats and fixed with 2.5% glutaraldehyde in PBS with a pH of 7. A small piece of the tissue was then embedded in paraffin before subjecting it to microtome sectioning. Hematoxylin and eosin (HE) were used for staining the tissues. The tissue response to nanofiber mats was evaluated from the coloration observed with a phase-contrast microscope.

Scanning Electron Microscopy (SEM). Nanofiber mat was placed on a stub and then coated with Au. The thickness of Au coat was about 15 nm. SEM images of nanofibers were obtained using a field emission scanning electron microspope (JSM-6330F, JEOL, Co. Ltd.) operating at an acceleration voltage of 5 kV of and an emission current of 12 μA. For estimating the average diameter of nanofibers, diameter was measured at more than 60 points on the printed SEM image.

Wide-Angle X-ray Diffraction (WAXD). WAXD patterns of nanofiber mats were acquired under ambient condition using Rigaku RINT-2500 system operating at 40 kV and 200 mA. Measurements were performed on a Bragg–Brentano type $2\theta/\theta$ goniometer in a reflection mode. Ni-filtered Cu Kα radiation ($\lambda = 0.15418$ nm) was collimated with a 1/2 deg divergence slit, 1/6 deg scatter slit and 0.15 mm receiving slit. Scans were performed three times in a 2θ range of 10–40° with a scan rate of 0.5°/min and 0.05° step.

Gel Permeation Chromatography (GPC) Analysis. The molecular weight analysis of the nanofiber mats was performed with gel-permeation chromatography at 40 °C, using a Shimadzu LC-10A GPC system equipped with a RID-10A refractive index detector and Shodex K-806 M and K-802 columns. Chloroform was used as the eluent at a flow rate of 0.8 mL min^{-1}. The calibration curve was prepared by using monodisperse polystyrene standards.

Results

Changes in the Appearance of Nanofiber Mats During Subcutaneous Implantation. Figure 1a,b shows SEM images of the PLLA and stereocomplexed PLA nanofibers, respectively. Both nanofibers possess similar morphology with the average fiber diameter of about 300 nm. However, totally different crystalline structure is formed in these nanofibers, as seen from the WAXD profiles in Figure 1c. PLLA nanofiber shows diffraction peaks at $2\theta = 15.1$, 16.5 (assigned to (110)/(200)), and 18.1° that are assigned to α-form homocrystal of PLA.[12] On the other hand, stereocomplexed PLA nanofiber showed diffraction peaks at $2\theta = 12.0$ (assigned to (110)), 20.8, and 24.1° that are assigned only to stereocomplex crystal of PLA.[12]

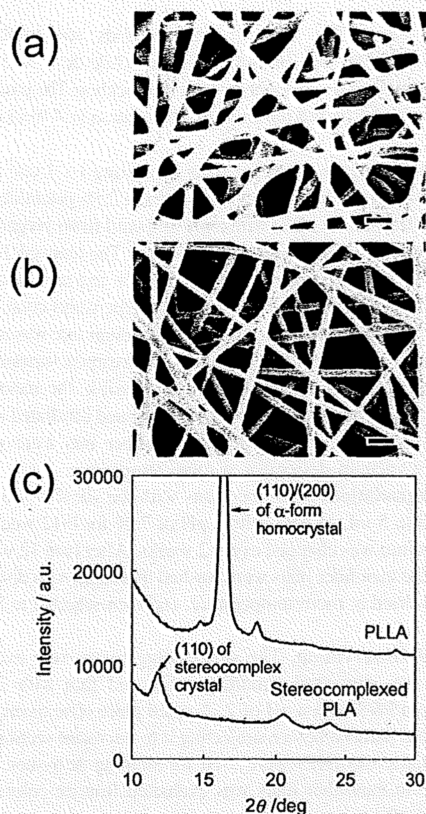

Figure 1. SEM images of (a) PLLA and (b) stereocomplexed PLA nanifibers and (c) wide-angle X-day diffraction patterns of PLLA and stereocomplexed PLA nanofibers. Scale bars = 1 μm. PLLA nanofiber shows diffraction peaks at 2θ = 15.1, 16.5 (assigned to (110)/(200)), and 18.1° that are assigned to α-form homocrystal of PLA. On the other hand, stereocomplexed PLA nanofiber showed diffraction peaks at 2θ = 12.0 (assigned to (110)), 20.8, and 24.1° that are aasigned only to stereocomplex crystal of PLA.

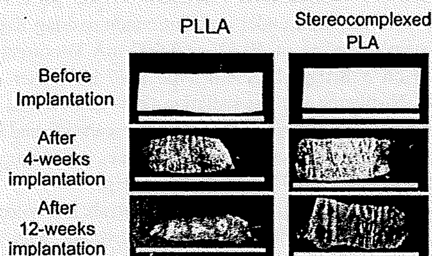

Figure 2. Bulk appearances of the nanofiber mats of PLLA and stereocomplexed PLA (a) before implantation, (b) after 4 weeks of implantation and (c) after 12 weeks of implantation. Scale bars = 3 cm.

This shows that the stereocomplexed PLA nanofiber consists of only the stereocomplex crystal and does not contain homocrystal of PLLA and PDLA at all.

The bulk appearances of the nanofiber mats were observed before and after removing the surrounding tissues. Figure 2 shows the photographs of nanofiber mats before and after 4 week and 12 week implantations, respectively. Significant reduction in the size of the PLLA nanofiber mat was recognized with the increasing period of implantation. In particular, the PLLA nanofiber mat after a 12 week implantation was densely covered with the surrounding tissues and only small fragments of the nanofibers mat were recovered. On the other hand, the stereocomplexed PLA nanofiber mat showed a less degree of the reduction in size than the PLLA nanofiber mat. This suggests that the in vivo degradation of the stereocomplexed PLA nanofiber mat occurs slower than the PLLA nanofiber mat.

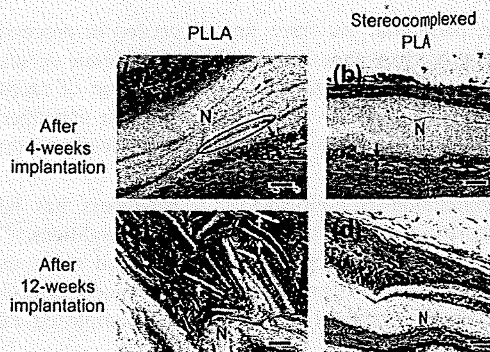

Figure 3. Histological images of PLLA and stereocomplexed PLA nanofibers before and after 4 weeks of implantation. (a) PLLA, before implantation; (b) stereocomplexed PLA, before implantation; (c) PLLA, after implantation; (d) stereocomplexed PLA, after implantation. Tissues were stained with hematoxylineosin. Nuclei of the inflammatory cells are stained blue. The width of inflammatory cells is indicated by the arrows and lines in (a) and (b). Ellipsoid region in (a) and white arrows in (c) indicate the infiltration of surrounding tissues and fragmented nanofibers, respectively. ST: surrounding tissues; N: nanofiber mats. Scale bars = 50 μm.

Histological Observation of Nanofiber Mats with the Surrounding Tissues. Histological observations of the nanofiber mats were performed to investigate the degree of inflammatory reactions and penetration of the surrounding tissues into the nanofiber mats. Figure 3 shows the phase contrast images of ultrathin sections of the explanted nanofiber mats stained by hematoxylin-eosin. The nuclei of inflammatory cells were stained blue by the hematoxylin dye and their presence is an indication of tissue response toward the implanted nanofiber mats. As indicated by the arrows and lines in Figure 3a, a thick layer of inflammatory cells was accumulated at the interface between the PLLA nanofiber mat and the surrounding tissues. In contrast, the layer of accumulated inflammatory cells was thinner for the stereocomplexed PLA nanofiber mat, as shown in Figure 3b. This indicates that the stereocomplexed PLA nanofiber mat causes smaller degree of inflammatory reactions than the PLLA nanofiber mat.

Furthermore, delamination (indicated by the ellipsoid in Figure 3a) occurred on the surface of the PLLA nanofiber mat, and hence, the infiltration of the surrounding tissues was observed. However, no infiltration of the surrounding tissues was observed for the stereocomplexed PLA nanofiber mat. After 12 weeks of implantation, while the PLLA nanofiber mat was significantly fragmented (white arrows indicate the fragmented nanofiber mat), the stereocomplexed PLA nanofibers retained the mat-like bulk morphology. These trends are well correlated with the bulk appearances of the nanofiber mats and support the observation that the in vivo degradation of the stereocomplexed PLA nanofiber mat proceeds slower than the PLLA nanofiber mat.

SEM Observation. SEM observation was performed for the nanofiber mats before and after 4 weeks and 12 weeks of implantation. Figure 4 shows the SEM images of nanofiber mats before implantation, after implantation and incubation at different periods of time. As for PLLA, cleavage of each strand of nanofiber occurred after 4 weeks. Furthermore, after 12 weeks, a decrease in the density of the nanofiber mat was observed. This is consistent with the histological image showing the fragmentation of the PLLA nanofiber mat. On the other hand, no cleavage of the stereocomplexed PLA nanofibers was observed even after 12 weeks of implantation.

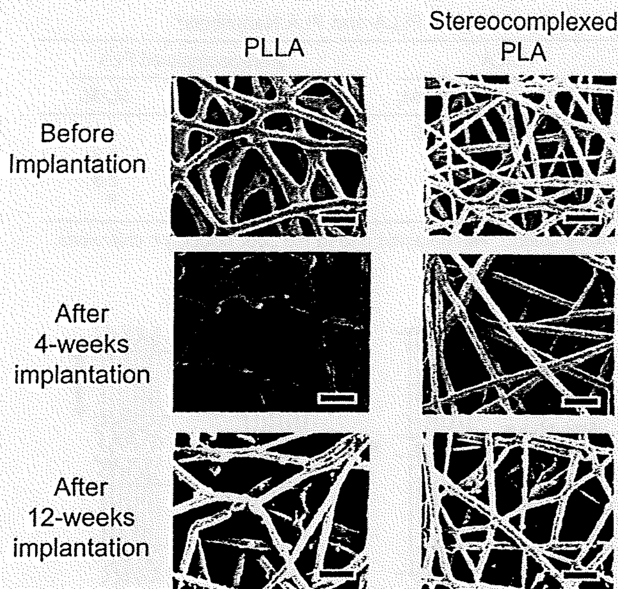

Figure 4. SEM images of PLLA (left) and stereocomplexed PLA (right) nanofibers. Upper row, before implantation; middle row, after 4 weeks of implantation; lower row, after 12 weeks of implantation. The surrounding tissues were removed by trypsin treatment. Scale bars = 1 μm.

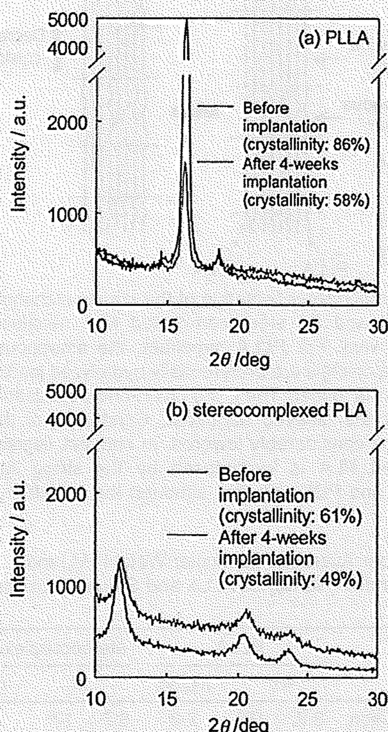

Figure 5. Wide-angle X-ray diffraction patterns of PLLA and stereocomplexed nanofibers before and after 4 weeks of implantation. PLLA nanofiber showed diffraction peaks at 2θ = 15.1°, 16.5°, and 18.1° that are assigned to homopolymer crystal of PLLA. On the other hand, stereocomplexed PLA nanofiber showed diffraction peaks at 2θ = 12.0, 20.8, and 24.1° that are assigned to stereocomplexed crystal. No diffraction peaks assigned to homopolymer crystal were observed in stereocomplexed PLA nanofiber.

Changes in Crystallinity. Figure 5 shows the WAXD patterns of the PLLA and stereocomplexed PLA nanofibers before and after 4 weeks of implantation. While the PLLA nanofiber showed diffractions that are assigned to the α-form crystal of PLA, the stereocomplexed PLA nanofiber showed diffractions assigned only to stereocomplexed crystal.[12] The crystallinity of both nanofibers was calculated as the ratio between the integrals of crystalline diffraction intensity and the total diffraction intensity. While the PLLA nanofiber showed considerable decrease in its crystallinity from 86 to 58%, the stereocomplexed PLA nanofiber showed a smaller decrease from 61 to 49%. These results show that the crystallinity of the stereocomplexed PLA is not so much lowered by implantation, while that of PLLA nanofiber significantly decreases. These results support the higher stability of stereocomplexed PLA nanofiber than PLLA nanofiber, as seen from visual inspection of the explanted nanofiber mat and the histological observation.

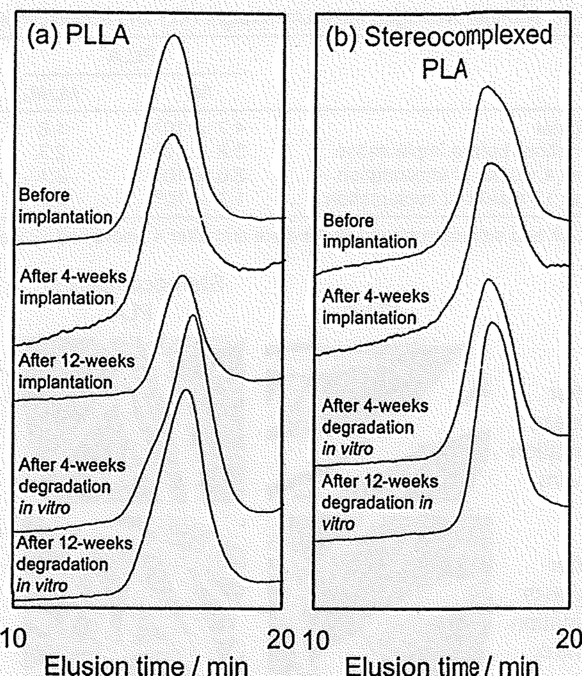

Figure 6. GPC elusion profiles of (a) PLLA and (b) stereocomplexed PLA nanofibers before and after implantation in vivo for 4 weeks and 12 weeks and before and after in vitro degradation for 4 weeks and 12 weeks.

GPC Analysis. The possibility of the cleavage of molecular chains during implantation, as suggested from SEM and WAXD data, was investigated by GPC analysis. The GPC elusion profiles are shown in Figure 6. Table 1 shows the number-averaged molecular weight, M_n, and the polydispersity index, M_w/M_n, of the PLLA and stereocomplexed PLA nanofibers before and after 4 weeks of implantation. Data for original PLLA are slso shown in Table 1. In the case of 12 weeks, GPC data of stereocomplexed PLA were not obtained because of its low solubility in chloroform. PLLA nanofiber showed a decrease in M_n during the implantation. In contrast, the M_n of stereocomplexed PLA nanofiber remained unchanged despite the decrease in M_w/M_n for 4 weeks of implantation. These results indicate that stereocomplexed PLA was not degradaded during implantation, while the PLLA chains in the nanofiber were considerably degraded. Additionally, in the case of the stereocomplexed PLA nanofiber, the extraction of low molecular weight fraction might occur during implantation.

In Vitro Degradation. To consider the results obtained from the in vivo experiment in terms of biocompatibility and bioabsorption, changes in the structure and properties of the nanofibers after in vitro incubation were investigated. As seen in Figure 7, both PLLA and stereocomplexed PLA nanofibers

Table 1. Number-Averaged Molecular Weight (M_n) and Polydispersity Index (M_w/M_n) of Original PLLA and PLA Nanofibers[a]

	PLLA		PDLA		stereocomplexed PLA	
	M_n	M_w/M_n	M_n	M_w/M_n	M_n	M_w/M_n
original	4.7×10^5	1.8	2.2×10^5	1.5		
nanofiber before implantation	3.8×10^5	2.3			8.7×10^4	3.3
after 4 weeks of implantation	3.0×10^5	2.4			8.6×10^4	2.3
after 12 weeks of implantation	1.7×10^5	2.3			[b]	[b]

[a] PLLA and stereocomplexed PLA before and after 4 weeks and 12 weeks of implantation. [b] Not obtained due to the poor solubility in chloroform.

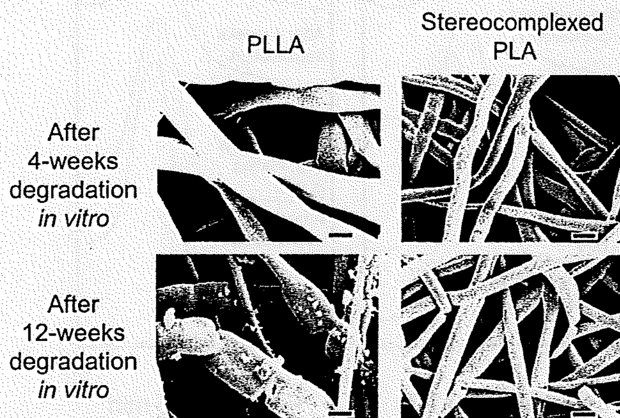

Figure 7. SEM images of PLLA (left) and stereocomplexed PLA (right) nanofibers after 4 weeks (upper) and 12 weeks (lower) in vitro degradation in PBS. Scale bars = 1 μm.

after in vitro incubation showed a considerable increase in the fiber diameter. This suggests that the significant swelling of the nanofibers occurred during the incubation. Interestingly, the stereocomplexed PLA nanofiber showed a smaller degree of swelling (from 300 to 600 nm) than the PLLA nanofiber (from 300 to 1200 nm). Because strong interaction works between molecular chains of PLLA and PDLA in the sterecomplexed PLA nanofiber, the swelling of the stereocomplexed PLA nanofiber might be suppressed.

GPC data of the nanofibers before and after in vitro degradation were also obtained, as shown in Figure 6b. The M_n and M_w/M_n estimated from the GPC curves are listed in Table 2. The M_n of stereocomplexed PLA was almost unchanged while that of PLLA showed a decrease from 3.8×10^5 to 1.8×10^5. These trends are consistent with the molecular weight data before and after the implantation in vivo as shown in Table 1.

The difference in the swelling behavior and molecular weight change in vitro between the stereocomplexed PLA and PLLA nanofibers may explain the results of the subcutaneous implantation in vivo in which the stereocomplexed PLA nanofiber showed smaller degree of absorption than the PLLA nanofiber.

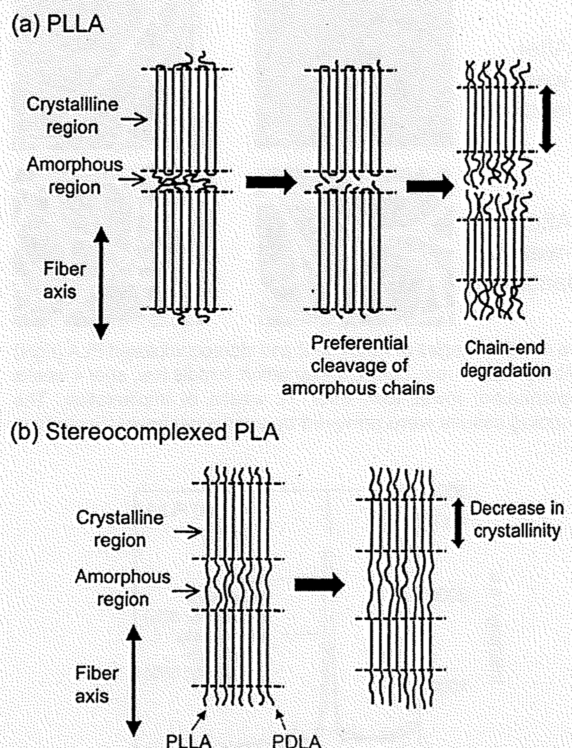

Figure 8. Schematic representation of the structural changes of (a) PLLA nanofiber and (b) stereocomplexed PLA nanofiber during implantation in vivo. For PLLA nanofiber, the amorphous chains between lamella crystals are preferentially hydrolyzed, leading to the cleavage of the nanofiber. Then, the chain-end degradation occurs at the edge of the cleaved nanofiber. Crystallinity of the PLLA nanofiber is thus considerably lowered. In contrast, degradation of stereocomplexed PLA is suppressed by the strong interaction between PLLA and PDLA chains, although the crystallinity slightly decreases.

Table 2. Number-Averaged Molecular Weight (M_n) and Polydispersity Index (M_w/M_n) of PLLA and Stereocomplexed PLA Nanofibers[a]

	PLLA		stereocomplexed PLA	
	M_n	M_w/M_n	M_n	M_w/M_n
before degradation	3.8×10^5	2.3	8.7×10^4	3.3
after 4 weeks of degradation	1.4×10^5	3.5	8.4×10^4	3.0
after 12 weeks of degradation	1.8×10^5	3.0	6.9×10^4	2.2

[a] Before and after 4 weeks and 12 weeks of degradation in vitro.

Discussion

Degradation Mechanism of PLLA and Stereocomplexed PLA Nanofibers In Vivo. A schematic representation of the degradation mechanism of the PLLA and stereocomplexed PLA nanofibers is shown in Figure 8. For the PLLA nanofiber, it is believed that the molecular chains in the amorphous region between lamella crystals are preferentially hydrolyzed due to the intracrystalline swelling. This leads to the cleavage of a nanofiber and a decrease in the molecular weight. Then the chain-end degradation at the edge of the cleaved nanofiber may occur and lead to the decrease in the crystallinity. The cleavage of nanofiber may facilitate the delamination and the subsequent fragmentation of the nanofiber mats and, consequently, the infiltration of surrounding tissues in the PLLA nanofiber mat. Inflammatory reaction at the early stage may be due to the acidic low-molecular-weight degradation products and fragmented nanofibers.

A different situation was observed for the stereocomplexed PLA nanofibers. It is supposed that a single stereocomplexed PLA nanofiber is composed of PLLA and PDLA chains aligned

in a side-by-side manner. Accordingly, it is well-known that molecular interaction between PLLA and PDLA chains is strong, leading to higher melting temperature. Such molecular arrangement may suppress the hydrolysis of molecular chains in vivo. Thus, the stereocomplexed nanofiber morphology is retained. As a result, inflammatory reaction is limited at the vicinity of the interfacial region between nanofiber mats and the surrounding tissues.

General Discussion. Physiological response of tissues against implanted foreign materials is one of the most significant subjects to be considered in the development of medical biomaterials. In the case of polymeric biomaterials, the degree of the tissue responses, such as inflammatory reactions, partly depends on the chemical structure and, as a consequence, surface hydrophilic nature of the polymers.[23] Additionally, for biodegradable polymers, the degree of tissue responses is affected by the degradability in vivo.[24] For example, poly(glycolic acid) that undergoes degradation in vivo generally in 2–4 weeks is known to cause acute inflammatory reaction as the degradation proceeds.[25] It is known that the hydrolysis by body fluids is the major mechanism contributing in vivo degradation of polymeric biomaterials. We have already shown that the degradation behavior of poly(hydroxyalkanoate)s (PHAs) in vivo are largely affected by the monomer composition.[26] Nanofiber scaffolds made from these PHAs, ranging from poly[(*R*)-3-hydroxybutyrate] to poly[(*R*)-3-hydroxybutyrate-*co*-97 mol %-4-hydroxybutyrate] lead to contrasted tissue responses. The tissue responses were well correlated with the degradability of each polymer scaffolds. The present study using nanofibers of PLLA and stereocomplexed PLA suggested the correlation between the degree of inflammatory reaction in vivo and the change in the bulk size of each nanofiber mats. The changes in bulk size of the nanofibers were correlated to the changes in the microscopic morphology, crystallinity, and molecular weight. All these factors give evidence that the stereocomplexed PLA nanofibers are more stable and thus provoke lower degree of inflammation in vivo than the PLLA nanofibers.

In general, inflammatory reaction is favored in the case where healing occurs in a short period of time. For example, inflammatory reaction stimulates and accelerates the regeneration of some kinds of epithelial tissues. On the other hand, in the case where healing requires a longer time, chronic inflammatory response is not favored. For example, suppression of the inflammatory responses against artificial vessel has significance for treatment of the circulatory organs that requires a period of more than half a year. From this viewpoint, our results show that the stereocomplexed PLA nanofibers are suitable for the purposes where the chronic inflammatory reaction should be avoided, for example, guided nerve regeneration or blood vessel augmentation. On the other hand, conventional PLLA nanofibers may be suitable for the rapidly bioresorbable materials, for example, wound healing patches. Such versatility of the biodegradability would expand the potential of PLAs as biomaterials.

Conclusion

Fiber morphology, crystallinity, and molecular weight of PLLA and stereocomplexed PLA nanofibers before and after implantation in vivo were investigated using SEM, WAXD, and GPC. The stereocomplexed PLA nanofiber retained its fiber morphology, crystallinity, and molecular weight after a 12 week implantation. On the other hand, the PLLA nanofiber showed breakdown of the fiber morphology and significant decrease in crystallinity and molecular weight. The degree of inflammatory reaction against the nanofibers in vivo was correlated to the degradation behavior. The larger stability against hydrolysis of stereocomplexed PLA nanofiber, attributed to the strong interaction between PLLA and PDLA chains in the nanofiber, was confirmed by in vitro degradation.

Acknowledgment. This work has been supported by a grant provided for Ecomolecular Research II in RIKEN Institute (The Institute of Physical and Chemical Research), Japan, and by a Grant-in-Aid from the Ministry of Education, Culture, Sports, Science and Technology, Japan (No. 19350075, to T.I.). We thank Ms. Noreen Fundador for the English correction of our manuscript.

References and Notes

(1) Langer, R.; Vacanti, J. P. *Science* **1993**, *260*, 920–926.
(2) Reneker, D. H.; Chun, I. *Nanotechnology* **1996**, *7*, 216–223.
(3) Morota, K.; Matsumoto, K.; Mizukoshi, T.; Konosu, Y.; Minagawa, M.; Tanioka, A.; Yamagata, Y.; Inoue, K. *J. Colloid Interface Sci.* **2004**, *279*, 484–492.
(4) Murugan, R.; Ramakrishna, S. *Tissue Eng.* **2006**, *12*, 435–447.
(5) Buchko, C. J.; Chen, L. C.; Shen, Y.; Martin, D. C. *Polymer* **1999**, *40*, 7397–7407.
(6) Zong, X.; Kim, K.; Fang, D.; Ran, S.; Hsiao, B. S.; Chu, B. *Polymer* **2002**, *43*, 4403–4412.
(7) Zong, X.; Ran, S.; Kim, K.-S.; Fang, D.; Hsiao, B.; Chu, B. *Biomacromolecules* **2003**, *4*, 416–423.
(8) Ikada, Y.; Tsuji, H. *Macromol. Rapid Commun.* **2000**, *21*, 117–132.
(9) Iwata, T.; Doi, Y. *Sen'i Gakkaishi* **2001**, *57*, 172–177.
(10) Ikada, Y.; Jamshidi, K.; Tsuji, H.; Hyon, S. H. *Macromolecules* **1987**, *20*, 904–906.
(11) Tsuji, H. *Macromol. Biosci.* **2005**, *5*, 569–597.
(12) Okihara, T.; Tsuji, M.; Kawaguchi, A.; Katayama, K.; Tsuji, H.; Hyon, S. H.; Ikada, Y. *J. Macromol. Sci., Part B: Phys.* **1991**, *30*, 119–140.
(13) Tsuji, H. *Polymer* **2000**, *41*, 3621–3630.
(14) Tsuji, H.; Suzuki, M. *Sen'I Gakkaishi* **2001**, *57*, 198-202.
(15) Tsuji, H.; Miyaushi, S. *Biomacromolecules* **2001**, *2*, 597–604.
(16) Takasaki, M.; Ito, H.; Kikutani, T. *J. Macromol. Sci., Part B: Phys.* **2003**, *42*, 57–73.
(17) Furuhashi, Y.; Kimura, Y.; Yamane, H. *J. Polym. Sci., Part B: Polym. Phys.* **2007**, *45*, 218–228.
(18) Tsuji, H.; Nakano, M.; Hashimoto, M.; Takashima, K.; Katsura, S.; Mizuno, A. *Biomacromolecules* **2006**, *7*, 3316–3320.
(19) Ishii, D.; Lee, W.-K.; Kasuya, K.-I.; Iwata, T. *J. Biotechnol.* **2007**, *132*, 318–324.
(20) Kim, K.; Yu, M.; Zong, X.; Chiu, J.; Fang, D.; Seo, Y.-S.; Hsiao, B. S.; Chu, B.; Hadjiargyrou, M. *Biomaterials* **2003**, *24*, 4977–4985.
(21) Zeng, J.; Chen, X.; Liang, Q.; Xu, X.; Jing, X. *Macromol. Biosci.* **2004**, *4*, 1118–1125.
(22) You, Y.; Min, B.-M.; Lee, S. J.; Lee, T. S.; Park, W. H. *J. Appl. Polym. Sci.* **2005**, *95*, 193–200.
(23) Wang, Y.-X.; Robertson, J. L.; Spillman, W. B.; Claus, R. O. *Pharm. Res.* **2004**, *21*, 1362–1373.
(24) Hasirci, V.; Lewandrowski, K.; Gresser, J. D.; Wise, D. L.; Trantolo, D. J. *J. Biotechnol.* **2001**, *86*, 135–150.
(25) Ceonzo, K.; Gaynor, A.; Shaffer, L.; Kojima, K.; Vacanti, C. A.; Stahl, G. A. *Tissue Eng.* **2006**, *12*, 301–308.
(26) Tan, H. Y.; Ishii, D.; Mahara, A.; Murakami, S.; Yamaoka, T.; Sudesh, K.; Samian, R.; Fujita, M.; Maeda, M.; Iwata, T. *Biomaterials* **2008**, *29*, 1307–1317.

BM8009363

Intracellular Enzyme-responsive Fragmentation of Nonviral Gene Carriers Leads to Polyplex Destabilization and Enhanced Transgene Expression

Tomoko Hashimoto,[1,2] Yoichi Tachibana,[1] Hisae Nozaki,[1] Osam Mazda,[3]
Takuro Niidome,[4] Akira Murakami,[2] and Tetsuji Yamaoka*[1]
[1]*Department of Biomedical Engineering, National Cardiovascular Center Research Institute, 5-7-1 Fujishirodai, Suita, Osaka 565-8565*
[2]*Department of Biomolecular Engineering, Kyoto Institute of Technology, Matsugasaki, Sakyo-ku, Kyoto 606-8585*
[3]*Department of Microbiology, Kyoto Prefectural University of Medicine, Kawaramachi-Hirokoji, Kamikyo-ku, Kyoto 602-8566*
[4]*Department of Applied Chemistry, Faculty of Engineering, and Center for Future Chemistry, Kyushu University, 744 Moto-oka, Nishi-ku, Fukuoka 819-0395*

(Received May 8, 2009; CL-090444; E-mail: yamtet@ri.ncvc.go.jp)

A novel cationic oligopeptide has been developed for bioprocessing-triggered nonviral gene delivery systems. Intracellular fragmentation of the carrier in response to endogenous enzyme, furin, led to destabilized polyplexes and enhanced transgene expression.

Various nonviral polymeric gene carriers have been recently proposed for effective gene transfer but are also known to inhibit the transcription efficiency in nuclei due to the strong polyplex compaction. The polyplex compaction is affected by various physical properties of carriers, such as hydrophobicity, hydrophilicity, and molecular weight (MW). Many researchers have been investigating the effect of carrier MW on transfection efficiency.[1–4] Godbey et al. reported that MW 70000 poly(ethyleneimine) (PEI) produced much higher expression levels than low MW PEI in cell culture because of better entry of polyplexes into the cells or stronger protection of pDNA.[1] On the other hand, Schaffer et al. reported that pDNA is dissociated from lower MW poly(L-lysine) more rapidly and that the weak interaction permits larger transcription rate in a cell-free system.[3] According to these findings, intracellular fragmentation of carriers is suspected to result in effective transfection because of the better entry of transgene and the higher transcription rate.

In this work, we designed oligopeptide-type nonviral carriers (Fur-oligopeptides) containing a cleavable sequence for intracellular proprotein convertase, furin. Furin is related to the processing of a wide variety of protein precursors within the secretory pathway and localized at trans-Golgi network, lysosome, and endosome of a broad range of mammalian cells.[5,6] It has been reported that furin recognizes the cleavage-site sequence Arg–X–X–Arg (R–X–X–R).[7] Especially, highly cationic Arg–X–(Lys/Arg)–Arg (R–X–(K/R)–R) is cleaved with 10-fold higher efficiency than R–X–X–R. Fur-oligopeptide, which has a repeating R–X–(K/R)–R sequence, is cationic enough to form polyplexes with nucleic acids electrostatically and to deliver nucleic acids into cells. Fur-oligopeptide is expected to be fragmented in an intracellular environment and lead to high transgene expression by releasing pDNA.

Fur-oligopeptides were synthesized by stepwise elongation of Fmoc amino acids on solid-phase resins. $(RKRKKR)_4C$ has seven cleavage sites.[8] $(RKRKRK)_4C$ is a control sequences without cleavage site. RKKR is a model peptide for the digested fragment.

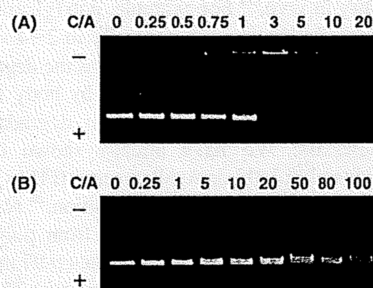

Figure 1. EtBr stained agarose gel (0.8%) electrophoresis of $(RKRKKR)_4C$/pT7-Luc (A) and RKKR/pT7-Luc (B) polyplexes at various C/A ratios.

$(RKRKKR)_4C$ formed polyplexes with pDNA completely at C/A ratio of 3 and above (Figure 1A). $(RKRKRK)_4C$ showed the same result (data not shown). On the other hand, RKKR formed polyplex at C/A ratio of higher than 100 (Figure 1B). Mascotti et al. calculated the equilibrium binding constant between oligolysine with various lengths and pDNA by measuring the thermodynamic extent of counter ion release resulted from the polyplex formation.[9] The equilibrium binding constant rapidly increased with increasing oligolysine length. The thermodynamic results support the large difference in polyplex-forming ability of $(RKRKKR)_4C$ (25mer) and RKKR (4mer). These results indicated that Fur-oligopeptide would lose the polyplex-forming ability and release the pDNA when fragmented in cells, which is expected to lead to high gene expression.

Polyplexes must be positively charged for better entry into cells. We measured ζ potential of $(RKRKKR)_4C$ or RKKR polyplexes. ζ Potentials of $(RKRKKR)_4C$ polyplexes were around +20 mV at a C/A ratio of 3, while RKKR polyplexes showed negative ζ potential up to a C/A ratio of 100 (data not shown). The ζ potential of $(RKRKKR)_4C$ polyplexes is similar to that of PEI/pDNA polyplexes and seems to be enough for gene delivery.[4]

Transient expressions of luciferase gene transfected with Fur-oligopeptides were evaluated. Polyplex solutions were incubated with COS-1 cells for 5 h in the presence of 200 µM chloroquine. Supernatants were removed and replaced with DMEM containing 10% FBS and then cells were cultured for 43 h. Luciferase count per second (CPS) of cells were measured using a luminometer. Obtained luciferase activities were divided by total

Copyright © 2009 The Chemical Society of Japan

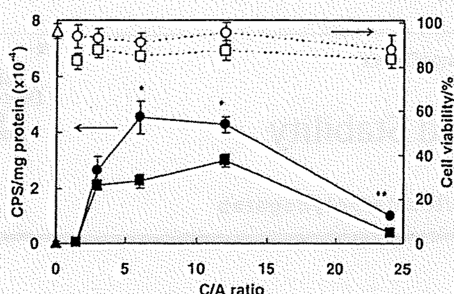

Figure 2. Transient luciferase expression (closed symbols) and cell viability (open symbols) in COS-1 cells transfected using $(RKRKKR)_4C$ (circles) and $(RKRKRK)_4C$ (squares) for 5 h in the presence of 200 µM chloroquine. (Triangles) represents the results for naked pCMV-Luc ($^*P < 0.01$, $^{**}P < 0.001$).

protein content of the cell lysates and expressed as CPS/mg protein (Figure 2). Cell viability was also assessed by the total protein in each cells. As is clearly shown, $(RKRKKR)_4C$ showed improved luciferase expression compared with a control $(RKRKRK)_4C$ with the same MW and amino acid composition. No cytotoxicity was observed in both cases. $(RKRKKR)_4C$ sequences in polyplexes is believed to be digested by intracellular furin, and this sequence-specific digestion brought about the polyplex destabilization.

We investigated the destabilization of Fur-oligopeptides/pDNA polyplexes in response to the digestion by furin in a cell-free system. Fur-oligopeptides were mixed with 200 ng pDNA in furin digestion buffer at $C/A = 5$ and incubated for 30 min. Five units of furin were added to 8 µL polyplex solutions and incubated for 1, 6, 12, and 24 h at 37 °C. Destabilization of polyplexes was evaluated by two experiments shown below. First, we perfomed anion-exchange assay with 0.5 equiv of potassium poly(vinyl sulfate) (PVS-K). When PVS-K was added to polyplex solutions, pDNA is replaced with PVS-K, and free pDNA is released. Reaction mixtures containing the free DNA were analyzed on EtBr-stained agarose gel (0.8%) electrophoresis. EtBr showed high fluorescence intensity by intercalating in free pDNA (Figure 3, Lane 1) but the intensity is completely suppressed when mixed with $(RKRKKR)_4C$/pDNA polyplexes because of their strong compaction (Figure 3, Lane 2). The fluorescence intensity was recovered by treating polyplexes with furin, and the intensity increased with the incubation time due to loosed compaction (Figure 3, Lane 3–6). Furthermore, release of free pDNA from digested polyplexes was observed, when the furin reaction time was longer than 12 h. Second, we evaluated the transription efficiency of the furin-treated polyplexes using an in vitro transcription/translation assay. Luciferase activity for $(RKRKKR)_4$/pT7-Luc polyplexes were increased to 30- and 100-fold after furin treatment for 1 and 6 h, respectively.[10] These results suggested that the enhanced gene expression shown in Figure 2 was resulted from the destabilization of highly compacted polyplex by intracellular furin digestion.

Katayama et al. reported polymeric carriers including substrates for protein kinase.[11] The substrate was phosphorylated by kinase, and then the charge of carriers decreased. As a result, the carriers lose polyplex-forming ability with pDNA, and GFP expression in NIH-3T3 cells was enhanced in response to the forskolin stimulation. However, since the positive charge density

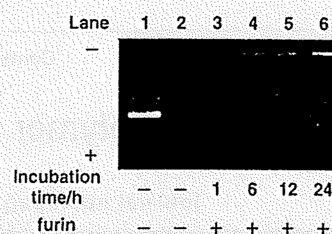

Figure 3. PVSK-induced disassembly of polyplexes treated with furin for 0, 1, 6, 12, and 24 h. Lane 1: free pCMV-Luc; lanes 2–6: $(RKRKKR)_4C$/pCMV-Luc polyplexes.

of this carrier is very low, the carrier cannot deliver pDNA into cells by itself and needs HVJ-E envelope. In contrast, $(RKRKKR)_4C$ can deliver pDNA into cells by itself and is fragmented to short peptides in response to intracellular furin. Other groups have reported biodegradable PEI derivatives.[12,13] These carriers might also facilitate intracellular release of pDNA from polyplexes, but remaining low MW PEI fragments are still non-biodegradable as is different from our Fur-oligopeptides.

In general, oligopeptide-type carriers have a high potential for useful gene carriers because various types of functional sequences such as receptor-binding sequences, NLS sequences, and digestive sequences can be combined. Increasing the MW of the carrier might be effective for pDNA delivery to cells[5] but higher MW carriers are reported to be more cytotoxic than the lower MW ones.[4] The optimum MW of Fur-oligopeptides are now studying.

In conclusion, Fur-oligopeptide has been newly developed as a gene carrier which is fragmented by intracellular furin, and the destabilized polyplexes are effectively transcibed in cells. This intracellular fragmentation of cationic carriers is a novel strategy for non-viral gene delivery.

This work was supported by Grants for Regional Science and Technology Promotion from the Ministry of Education, Culture, Sports, Science and Technology.

References and Notes

1 W. T. Godbey, K. K. Wu, A. G. Mikos, *J. Biomed. Mater. Res.* **1999**, *45*, 268.
2 P. Symonds, J. C. Murray, A. C. Hunter, G. Debska, A. Szewczyk, S. M. Moghimi, *FEBS Lett.* **2005**, *579*, 6191.
3 D. V. Schaffer, N. A. Fidelman, N. Dan, D. A. Lauffenburger, *Biotechnol. Bioeng.* **2000**, *67*, 598.
4 K. Kunath, A. V. Harpe, D. Fischer, H. Petersen, U. Bickel, K. Voigt, T. Kissel, *J. Controlled Release* **2003**, *89*, 113.
5 K. Hatsuzawa, M. Hosaka, T. Nakagawa, M. Nagase, A. Shoda, K. Murakami, K. Nakayama, *J. Biol. Chem.* **1990**, *265*, 22075.
6 S. S. Molloy, L. Thomas, J. K. VanSlyke, P. E. Stenberg, G. Thomas, *EMBO J.* **1994**, *13*, 18.
7 M. Hosaka, M. Nagahama, W. S. Kim, T. Watanabe, K. Hatsuzawa, J. Ikemizu, K. Murakami, K. Nakayama, *J. Biol. Chem.* **1991**, *266*, 12127.
8 T. Hashimoto, A. Murakami, T. Yamaoka, *Nucleic Acids Symp. Ser.* **2004**, *48*, 235.
9 D. P. Mascotti, T. M. Lohman, *Proc. Natl. Acad. Sci. U.S.A.* **1990**, *87*, 3142.
10 Supporting Information is available electronically on the CSJ-Journal Web site, http://www.csj.jp/journals/chem-lett/index.html.
11 Y. Katayama, K. Fujii, E. Ito, S. Sakakihara, T. Sonoda, M. Murata, M. Maeda, *Biomacromolcules* **2002**, *3*, 905.
12 C.-H. Ahn, S. Y. Chae, Y. H. Bae, S. W. Kim, *J. Control. Release* **2002**, *80*, 273.
13 G. P. Tang, H. Y. Guo, F. Alexis, X. Wang, S. Zeng, T. M. Lim, J. Ding, Y. Y. Yang, S. Wang, *J. Gene Med.* **2006**, *8*, 736.

Published on the web (Advance View) June 13, 2009; doi:10.1246/cl.2009.718

Polymer Degradation and Stability 94 (2009) 1349–1353

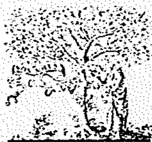

Contents lists available at ScienceDirect

Polymer Degradation and Stability

journal homepage: www.elsevier.com/locate/polydegstab

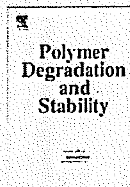

Self-assemblies of enzymatically degradable amphiphilic oligopeptides as nonviral gene carrier

Tomoko Hashimoto [a,b], Reiko Iwase [b,c], Akira Murakami [b], Tetsuji Yamaoka [a,b,*]

[a] Department of Biomedical Engineering, National Cardiovascular Center Research Institute, 5-7-1 Fujishirodai, Suita, Osaka 565-8565, Japan
[b] Department of Biomolecular Engineering, Kyoto Institute of Technology, Matsugasaki, Sakyo-ku, Kyoto 606-8585, Japan
[c] Department of Biosciences, Teikyo University of Science and Technology, 2525 Yatsusawa, Uenohara, Yamanashi 409-0193, Japan

ARTICLE INFO

Article history:
Received 25 April 2009
Received in revised form
25 May 2009
Accepted 28 May 2009
Available online 6 June 2009

Keywords:
Polymeric gene carrier
Self-assembly
Stability
Oligopeptide
Molecular weight

ABSTRACT

Novel biodegradable oligopeptide-type gene carriers composed of cationic residues (KRRRKRKRRRKRKRRC) and oligo leucine segments were developed. The amphiphilic carrier was found to form micelle-like assemblies in aqueous solutions, when the oligo leucine is 12 amino acids length (Pep-L12). NMR, CMC, and GPC analysis revealed their hydrophobic/cationic core/shell morphology. Hydrophobic interaction between leucines is thought to be the major driving force behind formations of assemblies. The transient expression of luciferase introduced to COS-1 cells using Pep-L12 below the CMC is as low as that by the control cationic peptides without leucine residue (Pep-L0), while improved transgene expression was observed in the case of Pep-L12 above CMC. The self-assembly raised the apparent molecular weight and gene transfection ability without loosening their low cytotoxicity. These results indicate that the amphiphilic oligopeptides are very promising materials as highly efficient and less toxic gene carriers.

© 2009 Elsevier Ltd. All rights reserved.

1. Introduction

Polymeric gene carriers are now extensively studied due to their high abilities to deliver and protect pDNA, but the polyplexes formed between the carriers and pDNAs are sometimes too highly compacted to be recognized by transcription factors in nucleus. Recently, the destabilization of the polyplexes by conjugating hydrophilic or hydrophobic segments to polymeric carriers has been reported [1–3]. However, excess modification of side chains results in the low resistance to DNase at the same time.

Effect of the carrier molecular weights (Mws) has been also being studied [4–8]. Recently, high potential of low Mw polymeric carriers was attracting great attention. Kunath et al. reported that low Mw PEI (5 kDa) was much less toxic than high Mw PEI (48 kDa), and reporter gene expression of 5 kDa PEI was 3.7-fold higher than 48 kDa PEI in various cell lines [6]. Breuning et al. compared PEIs with the Mw of 1–9 kDa and showed that the highest reporter gene expression was obtained at 5.6 kDa, with low cytotoxicity. Schaffer et al. reported higher gene expression for low Mw PLL (19 and 36 residues) than high Mw PLL (180 residues) because of effective *in vitro* transcription and easy pDNA release [4]. Taken together, low cytotoxicity and high DNA releasing ability of low Mw carries were important key features for the high potential gene carriers. On the other hand, low Mw carriers are pointed out to reduce cellular uptake [9] and decrease stability of polyplexes at the same time. Thus, a new type "low Mw carriers", which have low cytotoxicity, high cellular uptake, and adequate polyplex stability, would be more useful gene carriers.

In the present study, oligopeptide-type carriers were selected in order to reduce cytotoxicity and to induce the intracellularly digestible feature. Since the chemical chain elongation of cationic oligopeptide would increase the cytotoxicity, we tried to raise the apparent Mw of oligopeptide-type carriers by their self-assembly. Amphiphilic oligopeptides having cationic and hydrophobic sequences were then designed. Hydrophobic interactions between oligo leucine sequences make carriers form assemblies and increase the apparent Mw. Cationic sequences for interacting with pDNA include cleavable sequences (Arg-X-Lys/Arg-Arg (R-X-K/R-R)) by intracellular proprotein convertase, furin [10,11]. We have previously found that carriers including this cleavable sequences are enough cationic to form polyplexes with pDNA, and these polyplexes became destabilized if carriers were cleaved by furin [12]. Increased apparent Mw is expected to increase cellular uptake of the polyplex and the enhanced stability can be destabilized by furin cleavage resulting in the pDNA release in intracellular environments.

* Corresponding author at: Department of Biomedical Engineering, National Cardiovascular Center Research Institute, 5-7-1 Fujishirodai, Suita, Osaka 565-8565, Japan. Tel.: +81 6 6833 5012x2637; fax: +81 6 6835 5476.
E-mail address: yamtet@ri.ncvc.go.jp (T. Yamaoka).

0141-3910/$ – see front matter © 2009 Elsevier Ltd. All rights reserved.
doi:10.1016/j.polymdegradstab.2009.05.021

2. Experimental

2.1. Amphiphilic oligopeptides

We synthesized four oligopeptides by Fmoc-based solid phase method using 9050 plus PepSynthesizer (Applied Biosystems, CA, USA) and purified in the usual way. They are composed of cationic KRRRKRKRRRKRKRRC and hydrophobic oligo leucine segment with different lengths.

Oligopeptide solutions were analyzed by GPC (Shimadzu Corporation, Kyoto, Japan) which fitted with a combination of two columns of TSK gel G6000PWXL (21.5 mm I.D. × 300 mm length, Tosoh Corporation, Tokyo, Japan) and TSK gel G3000PWXL, RID-10A Refractive index detector, and SPD-M10A UV–VIS detector. Elution was carried out with 1/15 M phosphate buffer (pH 7.5) at 0.3 mL/min.

2.2. Critical micelle concentration (CMC) measurements

CMCs of oligopeptides in aqueous solution were measured on a RF5300PC (Shimadzu Corporation, Kyoto, Japan) using pyrene (Nacalai Tesque, Inc., Kyoto, Japan) as a hydrophobic region probe [13]. Five μL of pyrene solution in acetone at a concentration of 6×10^{-5} M was transferred into a vial and evaporated. Five hundred μL of oligopeptide solutions which ranging from 5.0×10^{-4}–1.5 g/L were added dropwise to make the pyrene concentration of 6.0×10^{-7} M, incubated at 65 °C for 3 h, and cooled down to the room temperature. Pyrene excitation spectra were measured with the slit widths of 5 and 1.5 nm for excitation and emission at an emission wavelength of 380 nm.

2.3. Polyplex formation with pDNA

pCMV-Luc and pT7-Luc (Promega corporation, WI, USA) were amplified to sufficient quantities by standard molecular biology techniques, and purified with a QIAGEN-tip 500 (QIAGEN K.K., Tokyo, Japan). Oligopeptide solutions were mixed with pDNA solutions at a given charge ratio which is the ratio of the number of cationic groups of oligopeptide to that of anionic group of pDNA (*C*/*A* ratio). The solutions were incubated for 30 min at 37 °C to allow the polyplex formation and analyzed on 0.8 wt% agarose gel in Tris–borate EDTA buffer at 100V for 30 min. pDNA was visualized by staining with 0.5 μg/mL ethidium bromide (EtBr, Sigma chemicals, St Louis, MO, USA).

2.4. In vitro *transfection*

COS-1 cells were grown in DMEM (Nissui, Tokyo, Japan) containing 10% fetal bovine serum (FBS) (Sigma chemicals, USA) at 37 °C under a 5% CO_2 atmosphere. COS-1 cells were seeded in 96 well culture plates at a density of 1×10^4 in 100 μL DMEM containing 10% FBS per well. After 24 h incubation, cells were washed with PBS, and 40 μL DMEM was added. Ten μL of polyplex solutions containing 100 ng pCMV-Luc at the concentration above or below CMC of Pep-L12 were poured gently to the wells. Fifty μL of 200 μM chloroquine solution was added (final concentration is 100 μM) and incubated for 5 h. Cells were washed with PBS and cultured for 43 h with DMEM containing 10% FBS at 37 °C in a 5% humidified CO_2 environment. The cells were washed with PBS, treated with the lysis buffer containing 1% Triton-X100, and incubated for 30 min at 37 °C. Cell lysate was diluted into luciferase assay solution containing 470 μM luciferin. The relative light units (RLU) of expressed luciferase were measured using ATP-300 Lumicounter (Advantec Toyo Kaisya, Ltd., Tokyo, Japan). Luciferase solutions at a known concentration were used for calibration. The protein concentration was determined by DC Protein Assay kit (Bio-Rad Laboratories, Hercules, CA, USA) using bovine serum albumin as a standard. The obtained luciferase expression (ng luciferase) was divided by total protein content of cell lysates and expressed as ng luciferase/mg protein.

Table 1
Sequences of amphiphilic oligopeptides.

Oligopeptide	Sequences and cleavage sites	Amino acid composition (K/R/L/C)
Pep-L0	H_2N-K-R-R-R-K-R*-K-R-R*-R-K-R*-K-R-R*-C-$CONH_2$	10/5/0/1
Pep-L4	H_2N-$(L)_4$-K-R-R-R-K-R*-K-R-R*-R-K-R*-K-R-R*-C-$CONH_2$	10/5/4/1
Pep-L8	H_2N-$(L)_8$-K-R-R-R-K-R*-K-R-R*-R-K-R*-K-R-R*-C-$CONH_2$	10/5/8/1
Pep-L12	H_2N-$(L)_{12}$-K-R-R-R-K-R*-K-R-R*-R-K-R*-K-R-R*-C-$CONH_2$	10/5/12/1

* represents the cleavage site of furin.

2.5. Cell-free assay system for luciferase expression

Fifteen μL of polyplexes ($C/A = 10$) were mixed with 12.8 μL of rabbit reticulocyte lysate mixtures (T_NT Coupled Reticulocyte Lysate Systems; Promega, WI, USA) and incubated with shake at rate of 300 rpm/min for 90 min at 30 °C. After transcription/translation assay according to the manufacture's protocol, luciferase activities were measured by the same method described in the above section.

3. Results and discussion

3.1. Self-assembly of amphiphilic carriers

Sequences and abbreviation of synthesized amphiphilic oligopeptides were shown in Table 1. GPC chart for each amphiphilic oligopeptide in phosphate buffer is shown in Fig. 1. Only Pep-L12 exhibited two peaks, while the other oligopeptides showed peak which is at the similar elution time to the second peak of Pep-L12. The first peak of Pep-L12 is considered to be attributed to the self-assembly of the Pep-L12 with the apparent higher Mw and the second peak corresponds to the unimer as low Mw as the other oligopeptides, Pep-L0, Pep-L4, and Pep-L8. These results indicated that only Pep-L12 forms micelle-like assemblies in aqueous solution.

Micelle-like assemblies can be confirmed by comparing ^1H NMR spectra in good solvents and water [14,15]. Protons in the core structure composed of the insoluble fractions do not provide sufficient NMR signals. Thus, self-assembly of oligopeptides was analyzed in DMSO and water. Leucine contents (X_{Leu}) in water and in DMSO were measured using the signal intensity at 0.8 ppm (CH_3 in leucine) and at 1.6 ppm (β-CH_2 and γ-CH in leucine, β, γ, and δ-CH_2 in lysine, β and γ-CH_2 in arginine, and SH in cysteine). The

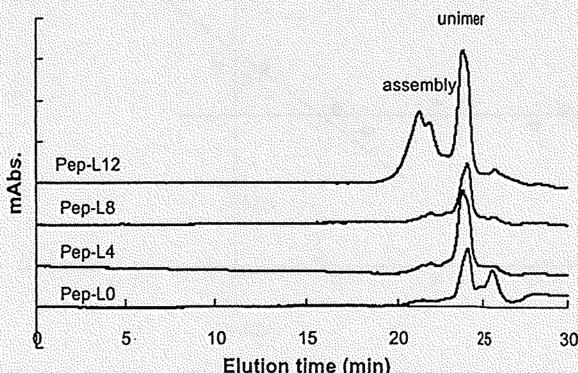

Fig. 1. GPC charts of Pep-LX (*X* = 0, 4, 8 and 12).

relative value of [X_{Leu} in water]/[X_{Leu} in DMSO] for Pep-L4 and Pep-L8 were 1.00 and 1.08, respectively, indicating that these oligopeptides has a same structure in both of medium. On the other hand, [X_{Leu} in water]/[X_{Leu} in DMSO] for Pep-L12 was 0.69, which strongly supports the oligo leucine/oligo cation core/shell structure of Pep-L12 in water.

3.2. CMC measurements

The excitation spectra of pyrene in oligopeptides solutions at various concentrations were measured. Fig. 2 demonstrates the intensity ratios ($I_{338.6}/I_{330.4}$) as a function of the logarithm of Pep-L12 concentration. As Pep-L12 concentration increased, the intensity ratio start increasing at a certain concentration, suggesting that pyrene molecules were incorporated into hydrophobic region upon assembly formation. CMC of Pep-L12 is determined from the crossover point was 0.16 g/L. This CMC is very high compared with reported CMC of other amphiphilic polymers [13,16]. This result suggested that Pep-L12 forms unstable assemblies resulting from weak hydrophobic interaction between leucine residues. In case of Pep-L8, a crossover point was not obtained. Hydrophobic interactions of Pep-L8 seem to be not strong enough to form assemblies in aqueous solution, which is in agreed with the GPC chart in Fig. 1. In addition, Pep-L12 assemblies were observed in AFM images above CMC (data not shown). While there were no assemblies at the lower concentration than CMC.

3.3. Polyplex formation

Fig. 3 shows the polyplex formation of the Pep-L12 at various *C/A* ratios. When Pep-L12 was mixed with pDNA, bands for free pDNA disappeared at the *C/A* ratio of 5, indicating that all pDNA form polyplexes with carriers. Concentrations of polyplex formation above and below CMC were same, indicating the polyplex forming ability of the micelle-like self-assembly of the Pep-L12 is same to that for Pep-L12 unimer. This phenomenon can be elucidated by the micelle-like architecture, which cationic residues are covering the hydrophobic core. The net amount of the cationic groups was then not significantly changed upon the self-assembly. Pep-L0 also formed polyplexes completely from *C/A* ratio of 5 similar to Pep-L12 (data not shown).

3.4. In vitro gene transfection

COS-1 cells were transfected with pCMV-Luc using Pep-L12 and Pep-L0 at various *C/A* ratio, and the transient expressions of luciferase gene were evaluated. Cell viabilities for Pep-L12 and Pep-L0 by after transfection procedure were higher than 80% (data not shown). In general, high Mw polycations have profound cell damages, but the cytotoxicity of Pep-L12 above CMC is low. As is shown in Fig. 4(b), both Pep-L0 and Pep-L12 oligopeptides did not work as gene carriers in the unimer forms. However, only Pep-L12 did lead to improved transgene expression as increasing *C/A* ratio when used as the micelle-like architecture above the CMC (Fig. 4(a)). Luciferase expression for Pep-L12 and Pep-L0 was 220.0 ± 68.0 and 19.3 ± 0.2 ng luciferase/mg protein at *C/A* ratio of 10, respectively. Under the same condition, we confirmed that the luciferase expression for oligoarginine (16 mer) was 2.4 ± 0.7 ng luciferase/mg protein at *C/A* ratio of 8 (data not shown). Luciferase expression for Pep-L12 was 100-fold higher than that for widely studied oligoarginine [17], indicating that Pep-L12 is a useful gene carrier.

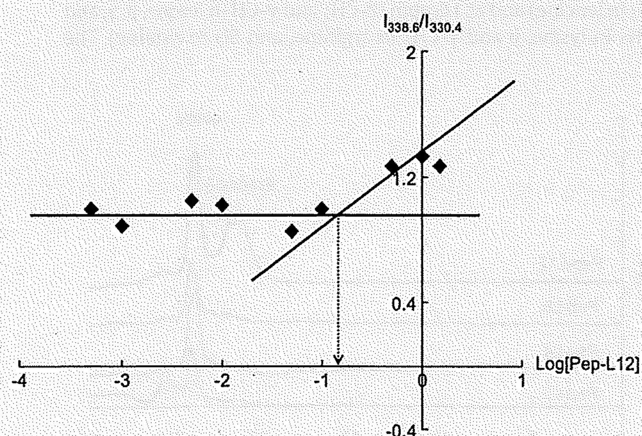

Fig. 2. $I_{338.6}/I_{330.4}$ in pyrene excitation spectra versus Pep-L12 concentration. CMC of Pep-L12 was 0.16 g/L.

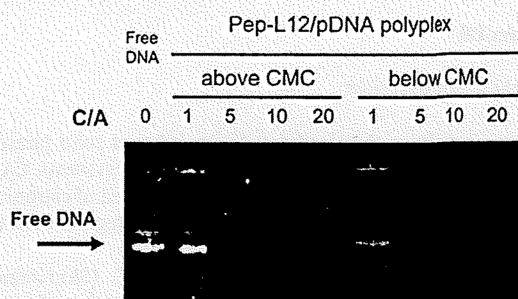

Fig. 3. Comparison of electrophoretic mobility profiles of Pep-L12 polyplexes. Polyplexes were analyzed at various *C/A* ratios on an agarose gel (0.8 wt%). Left five lanes represent polyplexes containing 200 ng pDNA above CMC and right four lanes are those containing 100 ng pDNA below CMC.

Possible reasons for improved transfection efficiency by Pep-L12 micell-like carrier is discussed below. First, pDNA uptake was improved because of the high apparent Mw. It was reported that cellular uptakes were increased as increasing in carrier Mw [9,18]. The second reason is the resistance of pDNA to DNase. We have studied the DNase I resistance of polyplexes for poly-L-lysine (from 15 to 1170 mer) or poly-L-arginine (from 70 to 650 mer) by incubating polyplexes with DNase I *in vitro*. As results, higher Mw polypeptide leads to the larger DNase resistance may be because of the large compaction of the polyplexes (data not shown).

Enhanced transcription is the third possible reason for the improved luciferase expression. We previously reported that a micelle-type polycation is superior to the linear-type polycation in gene transfer due to the enhanced transcription [2]. In addition, we found the enhanced gene expression of the linear-type oligopeptide composed of furin cleavage sequences in comparison to control sequences without cleavage sites [12]. These results indicated that the intracellular cleavage of the cationic residues in Pep-L12 self-assembly by intracellular furin enzyme might play a role in weakening the polyplex compaction by decreasing the charge density of the cationic micelle-like architecture.

3.5. Transcription/translation efficiency in cell-free system

To elucidate the reason for enhanced transgene expression, cell-free transcription/translation assay was performed using Pep-L0 and Pep-L12. The transcription efficiency of Pep-L12 was suppressed completely in comparison with free pT7-Luc, but Pep-L0 showed slightly residual transcription (Fig. 5). In general, polyplexes composed of high Mw polycation are strongly compacted and then hard to be transcribed. As is similarly, Pep-L12 forming micelle-like structure seems to suppress transcription in cell-free system. However, Pep-L12 successfully led to the transgene

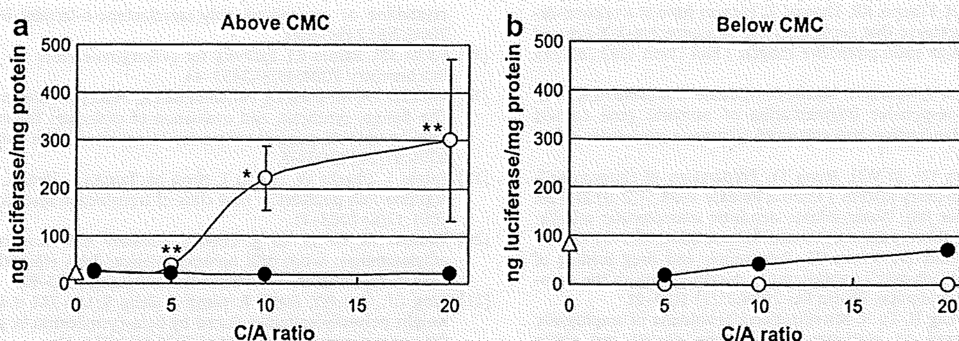

Fig. 4. Transient luciferase expression in COS-1 cells transfected using Pep-L0 (●) and Pep-L12 (○) in the presence of 100 μM chloroquine. (△) represents results for naked pCMV-Luc. Transfection assays were perfumed at above (a) or below (b) CMC of Pep-L12. (*$P < 0.01$, **$P < 0.05$.)

expression above CMC when evaluated in COS-1 system (Fig. 4), which indicates that the intracellular furin is able to associate with Pep-L12 somehow in cells.

In the present study, hydrophobic modification of the cationic gene carriers was proved to be effective. Pep-L12 formed hydrophobic/cationic core/shell morphology in aqueous solutions and lead to the enhanced gene expression *in vitro*. This type of core-shell structure should be energetically stable but the inverse structure has been also proposed. Futaki et al. reported that stearylated octaarginine forms polyplexes with the hydrophobic stearyl moieties at the outer surface and induces enhanced transgene expressions due to earlier endosomal escape. They expected that hydrophobic moieties contributed to interactions between polyplexes and cell membranes [19]. In our system, the leucine residues form core structure covered by the charged group and then it worked in the different mechanism.

In order to improve gene delivery efficiency with minimum cytotoxicity, several groups have reported the cross-linking of small PEIs with biodegradable linkage. Linked PEIs presented effective transgene expressions close to or higher than that offered by high Mw PEI (25 kDa) with reduced cytotoxicity [20,21]. Although low Mw PEI is much less cytotoxic than high Mw PEI, undegradable PEI remaining inside cells for a long period of time might interact with cell organelles and affect on cell functions [21]. On the other hand, oligopeptides would be understandably degraded if they remain inside cells after transfection. In this work, we designed novel oligopeptide-type carriers which showed high apparent Mw in aqueous solutions. Synthetic nonviral gene carriers composed of oligopeptides are thought to have potential of low cytotoxicity, enhanced cellular uptake and resistance to DNase. Further researches are necessary to clarify the intracellular behavior, physicochemical properties of polyplexes, such as degree of compaction and surface charge density.

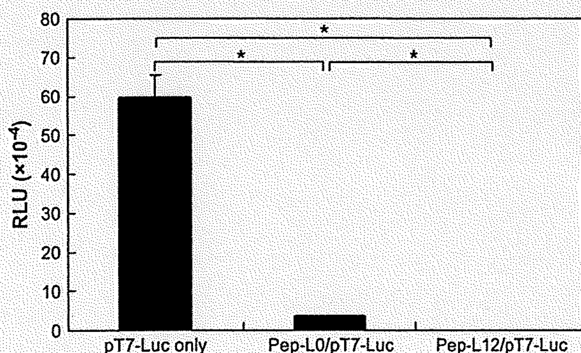

Fig. 5. Transcription efficiency determined by luciferase activity in *in vitro* transcription/translation system at *C/A* of 10. Polyplex formation was perfumed at a higher concentration than CMC of Pep-L12. (*$P < 0.0001$.)

4. Conclusions

A novel amphiphilic carrier Pep-L12 was synthesized by conjugating cationic sequences and hydrophobic sequences. Pep-L12 formed assemblies in aqueous solution at concentration above 0.16 g/L. Formations of assemblies brought about a dramatic increasing apparent Mw of carriers. Assemblies led enhanced transgene expression than linear carriers. Further analysis has to be done to design more effective self-assembly type gene carrier with low cytotoxicity.

Acknowledgements

We thank to Prof. Osam Mazda of Kyoto Prefectural University of Medicine for his great suggestion. This work was partly supported by Grants for Regional Science and Technology Promotion from the Ministry of Education, Culture, Sports, Science and Technology.

References

[1] Kimura T, Yamaoka T, Iwase R, Murakami A. Effect of physicochemical properties of polyplexes composed of chemically modified PL derivatives on transfection efficiency in vitro. Macromol Biosci 2002;2:437–46.
[2] Kitagawa T, Iwase R, Ishihara K, Yamaoka T, Murakami A. Facilitated disassembly of polyplexes composed of self-assembling amphiphilic polycations enhances the gene transfer efficacy. Chem Lett 2005;34(11):1478–9.
[3] Honore I, Grosse S, Frison N, Favatier F, Monsigny M, Fajac I. Transcription of plasmid DNA: influence of plasmid DNA/polyethylenimine complex formation. J Control Release 2005;107(3):537–46.
[4] Schaffer DV, Fidelman NA, Dan N, Lauffenburger DA. Vector unpacking as a potential barrier for receptor-mediated polyplex gene delivery. Biotechnol Bioeng 2000;67(5):598–606.
[5] Godbey WT, Wu KK, Mikos AG. Size matters: molecular weight affects the efficiency of poly(ethylenimine) as a gene delivery vehicle. J Biomed Mater Res 1999;45(3):268–75.
[6] Kunath K, VH A, Fischer D, Petersen H, Bickel U, Voigt K, et al. Low-molecular-weight polyethylenimine as a non-viral vector for DNA delivery: comparison of physicochemical properties, transfection efficiency and in vivo distribution with high-molecular-weight polyethylenimine. J Control Release 2003;89(1):113–25.
[7] Breunig M, Lungwitz U, Liebl R, Fontanari C, Klar J, Kurtz A, et al. Gene delivery with low molecular weight linear polyethylenimines. J Gene Med 2005;7(10):1287–98.
[8] Bettinger T, Carlisle RC, Read ML, Ogris M, Seymour LW. Peptide-mediated RNA delivery: a novel approach for enhanced transfection of primary and post-mitotic cells. Nucleic Acids Res 2001;29(18):3882–91.
[9] Varga CM, Tedford NC, Thomas M, Klibanov AM, Griffith LG, Lauffenburger DA. Quantitative comparison of polyethylenimine formulations and adenoviral vectors in terms of intracellular gene delivery processes. Gene Ther 2005;12(13):1023–32.
[10] Hosaka MNM, Kim WS, Watanabe T, Hatsuzawa K, Ikemizu J, Murakami K, et al. Arg-X-Lys/Arg-Arg motif as a signal for precursor cleavage catalyzed by furin within the constitutive secretory pathway. J Biol Chem 1991;266(19):12127–30.

[11] Molloy SSBP, Leppla SH, Klimpel KR, Thomas G. Human furin is a calcium-dependent serine endoprotease that recognizes the sequence Arg-X-X-Arg and efficiently cleaves anthrax toxin protective antigen. J Biol Chem 1992;267(23): 16396–402.
[12] Hashimoto T, Tachibana Y, Nozaki H, Mazda O, Niidome T, Murakami A, et al. Intracellular enzyme-responsive fragmentation of nonviral gene carriers leads to polyplex destabilization and enhanced transgene expression. Chem Lett, in press.
[13] Lee KY, Kwon IC, Kim YH, Jo WH, Jeong SY. Preparation of chitosan self-aggregates as a gene delivery system. J Control Release 1998;51(2-3):213–20.
[14] Liu M, Kono K, Frechet JMJ. Water-soluble dendritic unimolecular micelle: their potential as drug delivery agents. J Control Release 2000;65(1-2):121–31.
[15] Jette KK, Law D, Schmitt EA, Kwon GS. Preparation and drug loading of poly(ethylene glycol)-block-poly(ε-caprolactone) micelles through the evaporation of a cosolvent azeotrope. Pharm Res 2004;21(7):1184–91.
[16] Zhang J, Wang LQ, Wang H, Tu K. Micellization phenomena of amphiphilic block copolymers based on methoxy poly(ethylene glycol) and either crystalline or amorphous poly(caprolactone-b-lactide). Biomacromolecules 2006;7(9):2492–500.
[17] Fuchs SM, Raines RT. Pathway for polyarginine entry into mammalian cells. Biochemistry 2004;43(9):2438–44.
[18] Wender PA, Mitchell DJ, Pattabiraman K, Pelkey ET, Steinman L, Rothbard JB. The design, synthesis, and evaluation of molecules that enable or enhance cellular uptake: peptoid molecular transporters. Proc Natl Acad Sci U S A 2000;97(24):13003–8.
[19] Futaki S, Ohashi W, Suzuki T, Niwa M, Tanaka S, Ueda K, et al. Stearylated arginine-rich peptides: a new class of transfection systems. Bioconjug Chem 2001;12(6):1005–11.
[20] Thomas M, Ge Q, Lu JJ, Chen J, Klibanov AM. Cross-linked small polyethylenimines: while still nontoxic, deliver DNA efficiently to mammalian cells in vitro and in vivo. Pharm Res 2005;22(3):373–80.
[21] Tang GP, Guo HY, Alexis F, Wang X, Zeng S, Lim TM, et al. Low molecular weight polyethylenimines linked by beta-cyclodextrin for gene transfer into the nervous system. J Gene Med 2006;8(6):736–44.

AIChE

Antibody-Immobilized Column for Quick Cell Separation Based on Cell Rolling

Atsushi Mahara and Tetsuji Yamaoka
Dept. of Biomedical Engineering, Advanced Medical Engineering Center, National Cardiovascular Center Research Institute, Suita, Osaka, Japan 565-8565

DOI 10.1002/btpr.354
Published online November 13, 2009 in Wiley InterScience (www.interscience.wiley.com).

Cell separation using methodological standards that ensure high purity is a very important step in cell transplantation for regenerative medicine and for stem cell research. A separation protocol using magnetic beads has been widely used for cell separation to isolate negative and positive cells. However, not only the surface marker pattern, e.g., negative or positive, but also the density of a cell depends on its developmental stage and differentiation ability. Rapid and label-free separation procedures based on surface marker density are the focus of our interest. In this study, we have successfully developed an antiCD34 antibody-immobilized cell-rolling column, that can separate cells depending on the CD34 density of the cell surfaces. Various conditions for the cell-rolling column were optimized including graft copolymerization, and adjustment of the column tilt angle, and medium flow rate. Using CD34-positive and -negative cell lines, the cell separation potential of the column was established. We observed a difference in the rolling velocities between CD34-positive and CD34-negative cells on antibody-immobilized microfluidic device. Cell separation was achieved by tilting the surface 20 degrees and the increasing medium flow. Surface marker characteristics of the isolated cells in each fraction were analyzed using a cell-sorting system, and it was found that populations containing high density of CD34 were eluted in the delayed fractions. These results demonstrate that cells with a given surface marker density can be continuously separated using the cell rolling column. © 2009 American Institute of Chemical Engineers *Biotechnol. Prog.*, 26: 441–447, 2010
Keywords: cell separation, cell rolling, surface marker, antibody, CD34

Introduction

Because they do not lead to immunoreactions, tissue-derived stem cells have been the subject of much interest as an autologous source of stem cells.[1,2] The first important step in regenerative medicine using stem cells is to isolate a sufficient quantity of high purity stem cells in the clinically permitted period.[3,4] However, the isolation of homogeneous stem cells harvested from the body along with other mature cells is complicated procedure. Generally, stem cells are purified on the basis of their density,[5] size,[6] adhesion properties,[7] or surface maker patterns.[8–12] Although density gradient centrifugation and separation by size-sieving are relatively simple and easy to perform, they are not specific for stem cells. The most popular method for isolating mesenchymal stem cells (MSCs) is separation of the adherent cells on a plastic culture dish.[7] However, this method of cell isolation is also unsatisfactory for obtaining highly homogeneous stem cell populations.[2,13]

In contrast, an antibody-based strategy is much more effective and specific. Various cell surface markers have been found to be useful in identifying every type of stem cell. Once identified, stem cells can be isolated using fluorescence-activated cell sorting (FACS) or magnetic-activated cell sorting (MACS) systems. These strategies have been useful for separating target cells with an identified cell surface marker from unpurified cell populations.[14] For clinical stem cell therapy in cardiac revascularization, unpurified bone marrow cells or purified bone marrow CD133+ cells were injected into the infarct area; in these treatments, improvement in both blood flow and left ventricular function were observed.[13] However, contamination with other cell populations has also been described as a potential hurdles for clinical cell-therapy.

The types of surface markers expressed, as well as the level of marker expression, depend on the differentiation or developmental stage.[15,16] For example, the CD34 expression level of hematopoietic stem cells continuously decreases with developmental stage.[17] In myogenic progenitor cells, the expression level of CD34 changes during its differentiation into a myotube.[16] Marker density is a critical factor for stem cell separation; however, the widely used MACS system is not sensitive to marker density. One effective approach to this problem is to use a gate to set fluorescence intensity in FACS. The FACS system requires a rapid flow for cell sorting, and this affects the viability of sorting cells. Moreover, the cells thus obtained are contaminated with fluorescence- or magnetic bead-modified antibodies, which must be subsequently removed for safety.

Additional Supporting Information may be found in the online version of this article

Correspondence concerning this article should be addressed to T. Yamaoka at yamtet@ri.ncvc.go.jp.

© 2009 American Institute of Chemical Engineers